

University of Richmond

UR Scholarship Repository

Honors Theses

Student Research

2017

Differential equations models of pathogen-induced single- and multi-organ tissue damage

Fiona Lynch
University of Richmond

Follow this and additional works at: <https://scholarship.richmond.edu/honors-theses>



Part of the [Computer Sciences Commons](#), and the [Mathematics Commons](#)

Recommended Citation

Lynch, Fiona, "Differential equations models of pathogen-induced single- and multi-organ tissue damage" (2017). *Honors Theses*. 991.

<https://scholarship.richmond.edu/honors-theses/991>

This Thesis is brought to you for free and open access by the Student Research at UR Scholarship Repository. It has been accepted for inclusion in Honors Theses by an authorized administrator of UR Scholarship Repository. For more information, please contact scholarshiprepository@richmond.edu.

Differential Equations Models of Pathogen-Induced Single- and Multi-Organ Tissue Damage

Fiona Lynch
Honors Thesis¹

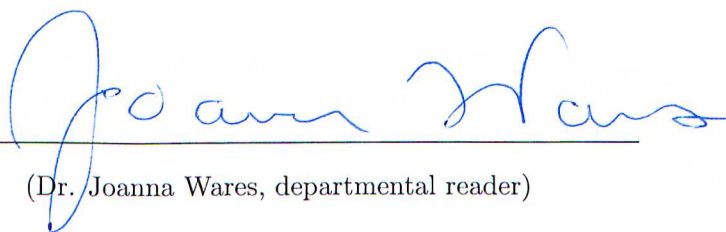
Department of Mathematics & Computer Science
University of Richmond

¹Under the direction of Dr. Lester F. Caudill, Jr.

The signatures below, by the thesis advisor, the departmental reader, and the honors coordinator
5 for mathematics, certify that this thesis, prepared by Fiona Lynch, has been approved, as to style
and content.



(Dr. Lester Caudill, thesis advisor)



(Dr. Joanna Wares, departmental reader)



(Dr. Van Nall, honors coordinator)

Chapter 1

Introduction

1.1 Background

The rise of antibiotic resistance has created a significant burden on healthcare systems around the world. Antibiotic resistance arises from the increased use of antibiotic drugs and antimicrobial agents, which kill susceptible bacterial strains, but have little effect on strains that have a mutation allowing them to survive antibiotic treatment, defined as “resistant” strains. With no non-resistant bacteria to compete for resources, the resistant bacteria thrives in this environment, continuing to reproduce and infect the host with an infection that does not respond to traditional antibiotic treatment.

The US Centers for Disease Control and Prevention estimates that in 2014, on a given day 1 in 25 hospital patients had at least one healthcare-acquired infection (HAI), defined as an infection secondary to the primary cause of hospitalization [18]. This places an incredible burden on hospital systems, with an annual estimated cost on US hospitals between \$28.4 and \$45 billion [49].

A number of strategies have been proposed to tackle the problem of antibiotic resistance, such as replacing broad-spectrum antibiotic (those that are generalized to kill non-specific strains of bacteria) treatments with pathogen-specific antibiotics and immunotherapies. However, testing these strategies with clinical experiments presents a significant time and financial burden, and are limited by ethical considerations for the human test subjects. Mathematical models, and their

implementation as computer simulation tools, can provide researchers with the means to simulate controlled experiments designed to assess the effectiveness of these strategies.

1.2 Starting Model

The present work builds upon a hybrid agent-based and mathematical model simulating the dynamics between pathogen and the host immune response to infection and antibiotic treatment in an ICU [5, 6]. The model has two levels: an agent-based inter-host model that models the interactions between hosts (patients and healthcare workers), with some probability of pathogen transfer for each interaction. At the in-host level, the model utilizes an ordinary differential equations (ODE) system to simulate interactions between the invading bacteria and the host's immune response over time.

The genesis of the present project lies in seeking to incorporate patient mortality into this hybrid HAI model. The efficacy of a given treatment option can be evaluated in its ability to reduce host death, making mortality rates an important metric to track in experiments. Thus, the goal of our project is to incorporate host death by pathogen infection into the model. Tissue damage and organ dysfunction, resulting largely from the body's inflammatory response to infection, is a primary cause of death in hospital-acquired infections [53], so we focus on incorporating tissue damage/dysfunction, defined as the proportion of functionality of a given organ, into the existing in-host model. While some infections are localized to a single organ, dysfunction in one organ can cause problems in other organ systems, exacerbating the existing challenges to the host's mortality. Also, since conditions such as septic shock (systemic organ failure resulting from an uncontrolled inflammatory response), are also prevalent in infected patients, we incorporate the effects of collateral and multiple organ failure into the model.

1.3 Previous Models

Previous attempts have been made to model the consequences of the pro-inflammatory response. Kumar et al [28] modeled pathogen-immune dynamics, including the feedback effects of two types

of pro-inflammatory mediators. Building on this work, Reynolds et al [45] incorporated inhibition of inflammation by anti-inflammatory mediators and include a non-specific tissue damage term. The work of Kheifetz et al [26] models the effects of pro-inflammatory mediators on the levels of C-reactive protein, a cellular marker of inflammation.

The mathematical models used in this research are just one component of a significantly larger simulation, and thus we attempt to keep the model uncomplicated to maintain computational efficiency while preserving biological accuracy. Incorporating one of these models would add, at minimum, three additional differential equations to the in-host model. Furthermore, none of these existing models include a concrete measure of tissue damage, which is required for our simulation. Thus, we construct a model incorporating the effects of the immune system's pro- and anti-inflammatory responses, including memory immune cells, and quantify tissue damage as a proportion of organ functionality. Here we present two mathematical models incorporating the damage caused by the body's pro-inflammatory response to infection, first in a single-organ system, and then in a sequential organ failure model that can be expanded to capture the interactions and dependencies of multiple organ systems.

In Chapter 2, we present our single-organ model with analysis and numerical demonstrations, and in Chapter 3 we present our multi-organ model with analysis and an experimental demonstration of sequential lung and kidney failure. In Chapter 4 we discuss our conclusions and future directions.

Chapter 2

Single Organ Damage Model

2.1 Biological Background

The body's response to infection is a highly complex process, some dynamics of which are still not fully understood. The goal of the immune response is to rid the body of antigens and restore the affected area to a healthy state through the pro-inflammatory response, but this response often comes with negative consequences in the form of local tissue damage.

The pro-inflammatory response is initiated by a “cytokine cascade,” in which cytokines, small proteins that release chemical signals to incite responses in other cells, are released in the infection site. The most prominent cytokines in the pro-inflammatory response, including Interleukin-1 (IL-1) and Tumor Necrosis Factor- α (TNF- α), are released in the infection site, initiating the local pro-inflammatory response [9]. The pro-inflammatory response is characterized by increased vascular permeability, increased leukocyte (white blood cell) adhesion to tissues, and the release of cytotoxic (cell-killing) neutrophil granules [11]. While the goal of the pro-inflammatory response is to remove antigens and necrotic cells from the infection site, this response can result in impaired function and cell death in healthy proximal tissues [57].

The pro-inflammatory action of the cytokine cascade is coupled with the release of anti-inflammatory cytokines (AIC), which help to mitigate the damage caused by the pro-inflammatory response. The AIC response has two primary mechanisms: IL-10, the predominant AIC in the immune response,

regulates the production of pro-inflammatory cytokines, while IL-22 promotes local tissue recovery ([11], [52], [39]).

When the pathogen threat has been sufficiently controlled, the immune system begins to return to its healthy state. Most of the immune responders targeted to the pathogen decay naturally, while some are transferred into the “memory” state. The memory state is characterized by a cell’s decreased size, lack of proliferation, and reduced metabolic rate [61]. If a secondary infection by the same pathogen is detected, these cells serve to quickly activate local cytotoxic immune cells, in order to more quickly and effectively mount an immune response to the infection, a process known as the “immunological memory” property [13].

Our mathematical model of damage to a single organ caused by the immune response to a pathogen captures the dynamics of both pro- and anti-inflammation triggered by the immune response to pathogen, as well as the transfer of activated immune cells to the memory state in the case of pathogen clearance.

2.2 Proposed Model

2.2.1 Starting Model

The starting in-host differential equations model for this project is from Caudill ([4]), and models the change in concentration of pathogens P and active immune responders I over time, t .

$$\frac{dP}{dt} = \frac{aP}{\lambda} - \frac{bPI}{\lambda(E+P)}, \quad P(0) = P_0, \quad (2.1)$$

$$\frac{dI}{dt} = \frac{\sqrt{\lambda}cP}{K+P} + \frac{\sqrt{\lambda}qI}{B+I} - \frac{rI}{\lambda}, \quad I(0) = I_0. \quad (2.2)$$

The terms on the right hand side of (2.1) represent natural pathogen growth and pathogen removal by immune responders, respectively. The terms in (2.2) represent the recruitment of immune cells when the presence of a pathogen is detected, additional recruitment effects by activated immune responders (a process known known as *autocatalysis*), and natural immune cell decay, respectively. The dimensionless parameter λ is known as the immunocompetence parameter (or

IC-parameter), and represents an individual host's level of immunocompetence, with a large λ representing a stronger immune response. As demonstrated in [4], the model (2.1)-(2.2) has the following key properties:

- positivity of solutions, i.e. if $P_0 > 0$ and $I_0 > 0$, then, for every $t > 0$, $P(t) \geq 0$ and $I(t) \geq 0$,
- the existence, under mild conditions on the coefficients of (2.1)-(2.2), of two constants $0 < L_1 < L_2$, for which

$$- 0 < \lambda < L_1 \implies \lim_{t \rightarrow \infty} P(t) = +\infty, \text{ i.e. the pathogen grows unboundedly;}$$

$$- L_1 < \lambda < L_2 \implies 0 < \lim_{t \rightarrow \infty} P(t) < \infty, \text{ i.e. the pathogen growth is controlled, but the pathogen is not eliminated;}$$

$$- L_2 < \lambda \implies \lim_{t \rightarrow \infty} P(t) = 0, \text{ i.e. the pathogen is eventually eliminated.}$$

So, by varying the IC-parameter, otherwise identical patients can experience all three of the potential treatment outcomes, indicating that the IC-parameter is an accurate measure of immune strength.

- the immunologic memory property, in which a host that has previously cleared the pathogen invasion is able to mount a faster, stronger immune response upon secondary infection by the same pathogen.

In order to model pathogen-induced tissue damage, it is necessary to modify the existing pathogen-immune model. As part of the immunologic memory property, the model (2.1)-(2.2) predicts that upon pathogen clearance, a positive number of immune responders remain in the host. This presents an issue, as the ‘‘autocatalysis term’’ would result in continued recruitment of additional immune responders despite the cleared pathogen threat. Thus, we modify the autocatalysis term of (2.2) to incorporate a dependence on the presence of a pathogen, which prevents active immune responders from recruiting additional active immune responders when the pathogen threat has been cleared. We also modify the pathogen growth term to indicate logistic growth with a finite carrying capacity, P_{max} , resulting in the following modified model:

$$\frac{dP}{dt} = \frac{aP}{\lambda} \left(1 - \frac{P}{P_{max}} \right) - \frac{bPI}{\lambda(E+P)}, \quad P(0) = P_0, \quad (2.3)$$

$$\frac{dI}{dt} = \sqrt{\lambda} \left(c + \frac{qI}{B+I} \right) \frac{P}{K+P} - \frac{rI}{\lambda}, \quad I(0) = I_0. \quad (2.4)$$

2.2.2 Memory Immune Response

Next, we differentiate the model's immune responder cells into two categories: active immune cells, which are actively combatting the pathogen threat, and memory immune cells, which have been converted into an inactive state to reinitiate an immune response in the case of a secondary infection. (These dynamics are illustrated in Figure 2.1.) We re-task the variable I to represent the active immune responders and we introduce a new variable, Q to denote memory immune cells.

The updated pathogen-immune dynamics from Fig. 2.1 are expressed in Equations (2.5)-(2.7):

$$\frac{dP}{dt} = (a) - (b), \quad (2.5)$$

$$\frac{dI}{dt} = (c) + (d) + (e) - (f) - (g), \quad (2.6)$$

$$\frac{dQ}{dt} = (g) - (h). \quad (2.7)$$

The terms (a), (b), (c), (e), and (f) remain the same as the model (2.3)-(2.4). As memory immune cells do not reproduce, the terms in (2.7) indicate only the transfer of active immune cells to the memory state when pathogen concentrations are low (g) and natural cell decay (h). The activation of quiescent immune cells to the active state is represented by (d). The bouncing arrow indicates a dependency on both Q and P being non-zero for this transfer to occur, as there must be both a pathogen threat and existing memory cells for the immunologic memory property to apply. The following 3×3 ODE system of pathogen, memory immune cell, and pathogen immune cell dynamics follows from (2.5)-(2.7):

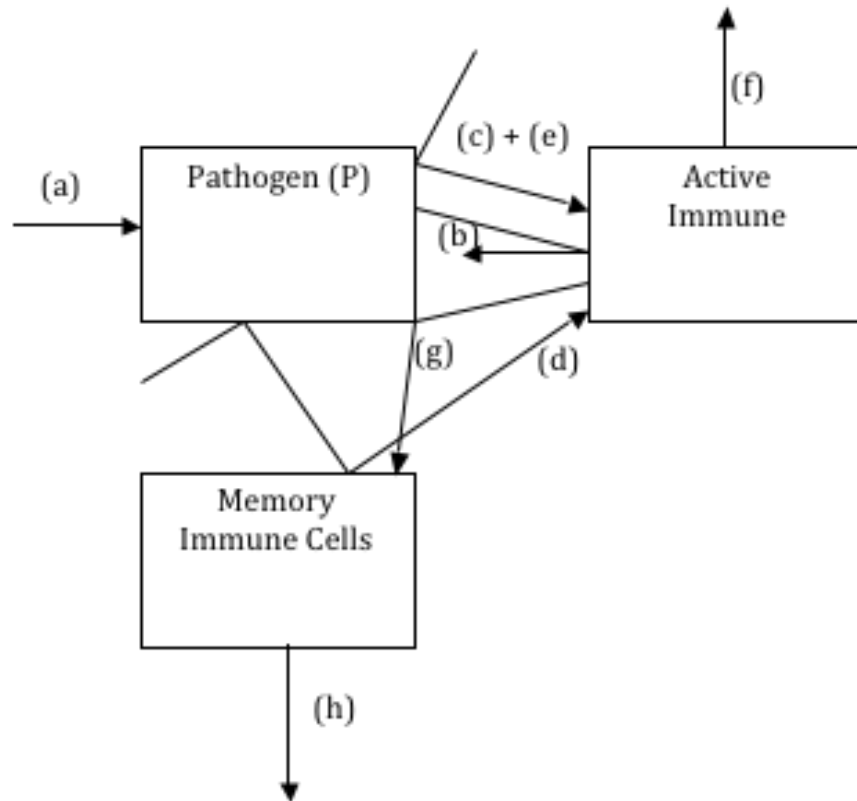


Figure 2.1: Box diagram of the pathogen-immune model incorporating active (I) and memory (Q) immune cells.

$$\frac{dP}{dt} = \frac{aP}{\lambda} \left(1 - \frac{P}{P_{max}} \right) - \frac{bPI}{\lambda(E+P)}, \quad P(0) = P_0, \quad (2.8)$$

$$\frac{dI}{dt} = \sqrt{\lambda} \left(c + \nu Q + \frac{qI}{B+I} \right) \frac{P}{K+P} - \frac{rI}{\lambda} - uIe^{-\chi P}, \quad I(0) = I_0, \quad (2.9)$$

$$\frac{dQ}{dt} = uIe^{-\chi P} - \kappa Q, \quad Q(0) = Q_0, \quad (2.10)$$

2.2.3 Anti-Inflammatory Mediators

As described in 2.1, AIC's such as IL-10 and Il-22 are critical in mitigating the damage caused by the pro-inflammatory response to infection. Since these are produced as part of the larger cytokine cascade, the concentration of AICs is dependent on the overall size of the immune response, and thus we denote AICs with the term $C(I)$, a function of the active immune cells. Since, for small concentrations of active immune responders, the inhibitory effects of AICs are negligible, while at large concentrations the AIC population will be proportional to the active immune responder population, we propose the following continuous piecewise function:

$$C(I) = \begin{cases} 0 & \text{if } I \leq I_c - \delta_I \\ \frac{\mu}{4\delta_I} (I - (I_c - \delta_I))^2 & \text{if } I_c - \delta_I < I \leq I_c + \delta_I \\ \mu(I - I_c) & \text{if } I > I_c + \delta_I \end{cases} . \quad (2.11)$$

When the concentration of activated immune responders surpasses a threshold value, I_c , the AICs are produced at a rate proportional to the number of active immune responders, and below this level the concentration is 0. When I is in the δ_I -neighborhood of I_c (for a small, positive δ_I), we model the concentration of AICs with a connecting polynomial function in order to ensure continuity.

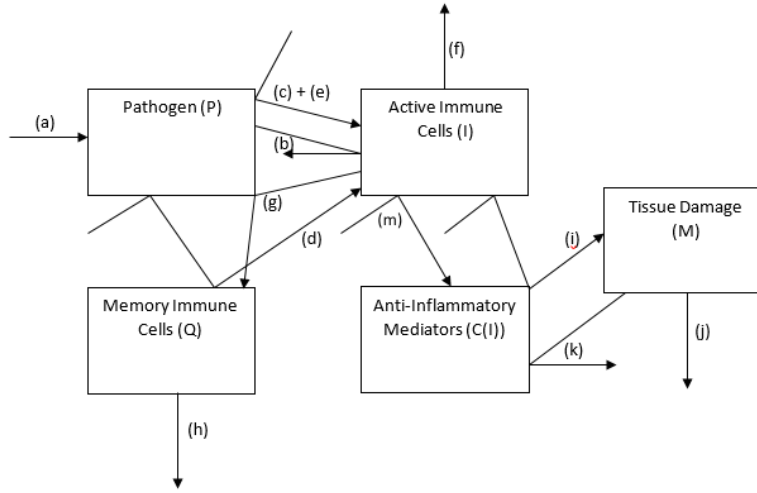


Figure 2.2: Box diagram of the dynamics of tissue damage caused by the active immune response, and regulated by anti-inflammatory immune cells ($C(I)$).

2.2.4 Tissue Damage

Building on the system described by (2.8) - (2.11) and the dynamics described in Fig. 2.2, we can develop our tissue damage model. With the terms described by arrows (a), (b), (c), (d), (e), (f), (g), (h), and (m) in Fig. 2.2 the same as in sections 2.2.2 and 2.2.3, we can introduce our tissue damage variable, M , where:

$$\frac{dM}{dt} = (i) - (j) + (k). \quad (2.12)$$

M represents the proportion of organ dysfunction, with $M = 0$ indicating a fully functional organ and $M = 1$ indicating an organ with total tissue dysfunction. Equation (2.12) represents the rate of damage to the tissue, with damage resulting from the presence of active immune responders and regulated by the presence of AICs (i). This model assumes all tissue to be fully recoverable, and thus tissue repair is modeled with a baseline rate (j), with enhanced recovery in the presence of AICs (k).

Thus, our final model of single-organ inflammatory tissue damage due to a pathogen is as

follows:

$$\frac{dP}{dt} = \frac{aP}{\lambda} \left(1 - \frac{P}{P_{max}}\right) - \frac{bPI}{\lambda(E+P)}, \quad P(0) = P_0, \quad (2.13)$$

$$\frac{dI}{dt} = \sqrt{\lambda} \left(c + \nu Q + \frac{qI}{B+I}\right) \frac{P}{K+P} - \frac{rI}{\lambda} - uIe^{-\chi P}, \quad I(0) = I_0, \quad (2.14)$$

$$\frac{dQ}{dt} = uIe^{-\chi P} - \kappa Q, \quad Q(0) = Q_0, \quad (2.15)$$

$$\frac{dM}{dt} = \frac{kI}{A+C(I)} - \left(\alpha + \frac{\gamma C(I)}{N+C(I)}\right) M, \quad M(0) = M_0, \quad (2.16)$$

where,

$$C(I) = \begin{cases} 0 & \text{if } I \leq I_c - \delta_I \\ \frac{\mu}{4\delta_I} (I - (I_c - \delta_I))^2 & \text{if } I_c - \delta_I < I \leq I_c + \delta_I \\ \mu(I - I_c) & \text{if } I > I_c + \delta_I \end{cases} . \quad (2.17)$$

2.3 Model Analysis

Given that the IVP system (2.13)-(2.16) is intended to model the interactions between four physical quantities, it is important to verify that solutions of this system cannot become negative.

Theorem 1. *If $P_0, I_0, Q_0, M_0 > 0$, then the solution $(P(t), I(t), Q(t), M(t))$ of the IVP system (2.13)-(2.16) must satisfy $P(t) > 0, I(t) > 0, Q(t) > 0$, and $M(t) > 0$ for every $t > 0$.*

Proof. Assume (by way of contradiction) that, for some $t > 0$, at least one of these inequalities hold: $P(t) \leq 0, I(t) \leq 0, Q(t) \leq 0$, or $M(t) \leq 0$. Then, there exists a first t -value, t_0 , for which $P(t_0)I(t_0)Q(t_0)M(t_0) = 0$. Then, since $P(t) \geq 0, I(t) \geq 0, Q(t) \geq 0$ and $M(t) \geq 0$ for $0 \leq t \leq t_0$, the four functions

$$\begin{aligned}\psi_P(t) &\equiv \frac{a}{\lambda} \left(1 - \frac{P}{P_{max}} \right) - \frac{b}{\lambda} \frac{I(t)}{E + P(t)} \\ \psi_I(t) &\equiv \sqrt{\lambda} \frac{q}{B + I(t)} \frac{P(t)}{K + P(t)} - \frac{r}{\lambda} - ue^{-\chi P(t)} \\ \psi_Q(t) &\equiv -\kappa \\ \psi_M(t) &\equiv - \left(\alpha + \frac{\gamma C(I(t))}{N + C(I(t))} \right)\end{aligned}$$

are each continuous on $0 \leq t \leq t_0$, and have finite absolute minima Λ_P , Λ_I , Λ_Q , and Λ_M , respectively, on this interval. So,

$$\frac{dP}{dt} = \psi_P(t)P \geq \Lambda_P P,$$

$$\frac{dI}{dt} = \sqrt{\lambda}(c + \nu Q) \frac{P}{K + P} + \psi_I(t)I \geq \Lambda_I I,$$

$$\frac{dQ}{dt} = uIe^{-\chi P} + \psi_Q(t)Q \geq \Lambda_Q Q,$$

$$\frac{dM}{dt} = \frac{kI}{A + \rho C(I)} + \psi_M(t)M \geq \Lambda_M M.$$

Consequently, the Mean Value Theorem yields

$$P(t_0) \geq P_0 e^{\Lambda_P t_0} > 0,$$

$$I(t_0) \geq I_0 e^{\Lambda_I t_0} > 0,$$

$$Q(t_0) \geq Q_0 e^{\Lambda_Q t_0} > 0,$$

$$M(t_0) \geq M_0 e^{\Lambda_M t_0} > 0,$$

which contradicts the assumption that $P(t_0)I(t_0)Q(t_0)M(t_0) = 0$. Thus, $P(t) > 0$, $I(t) > 0$, $Q(t) > 0$, and $M(t) > 0$ for every $t > 0$. \square

Given our interpretation of $M(t)$ as the proportion of the host's tissue that is damaged at time t , we must establish conditions on our model to ensure that $0 \leq M(t) \leq 1$ for all $t > 0$. Before doing so, it will be convenient to prove two simple lemmas.

Lemma 2. *If $\sigma > 0$ and $0 \leq y_0 \leq 1$, then any continuously differentiable function $y(t)$ that satisfies the differential inequality*

$$\frac{dy}{dt} \leq \sigma(1 - y), \quad y(0) = y_0, \quad t > 0,$$

must also satisfy $y(t) \leq y_0$, $\forall t > 0$.

Proof. The initial value problem

$$\frac{d\omega}{dt} = \sigma(1 - \omega), \quad \omega(0) = y_0,$$

has solution $\omega(t) = 1 - (1 - y_0)e^{-\sigma t}$. It then follows from the Mean Value Theorem that a solution $y(t)$ of the differential inequality must satisfy, for each $t > 0$,

$$y(t) \leq \omega(t) = 1 - (1 - y_0)e^{-\sigma t} \leq 1 - (1 - y_0) = y_0.$$

So, $y(t) \leq y_0 \forall t > 0$. \square

Lemma 3. *Consider the auxiliary function $\phi(x) = \frac{\gamma\mu}{k} \left(\frac{A + \mu x}{N + \mu x} \right)$, with $\gamma, \mu, k, A, N > 0$. If $\frac{\gamma\mu}{k} \min \left\{ \frac{A}{N}, 1 \right\} \geq 1$, then $\phi(x) \geq 1 \forall x > 0$.*

Proof. A direct calculation reveals that ϕ is an increasing function of x if $N > A$, and decreasing if $N \leq A$. So, if $N > A$, we have, for any $x > 0$,

$$\phi(x) \geq \inf_{x \geq 0} \phi(x) = \phi(0) = \frac{\gamma\mu A}{kN} \geq \frac{\gamma\mu}{k} \min \left\{ \frac{A}{N}, 1 \right\} \geq 1.$$

Likewise, if $N \leq A$, we have, for any $x > 0$,

$$\phi(x) \geq \inf_{x>0} \phi(x) = \lim_{x \rightarrow \infty} \phi(x) = \frac{\gamma\mu}{k} \geq \frac{\gamma\mu}{k} \min \left\{ \frac{A}{N}, 1 \right\} \geq 1.$$

Thus, $\phi(x) \geq 1 \forall x > 0$. □

Theorem 4. *If $M_0 \leq 1$, $\frac{kI_c}{\alpha A} \leq 1$, and $\frac{\gamma\mu}{k} \min \left\{ \frac{A}{N}, 1 \right\} \geq 1$, then the solution $M(t)$ of equation (2.16) satisfies $0 \leq M(t) \leq 1 \forall t > 0$.*

Proof. First, note that the result $0 \leq M(t)$ is an immediate consequence of Theorem 1. For the other inequality, we first consider the case where $I \leq I_c$, in which (2.16) becomes

$$\frac{dM}{dt} = \frac{kI}{A} - \alpha M. \quad (2.18)$$

Since $\frac{kI_c}{\alpha A} \leq 1$, we have $\frac{kI}{A} \leq \alpha$, so (2.18) yields

$$\frac{dM}{dt} \leq \frac{kI_c}{A} - \alpha M \leq \alpha - \alpha M = \alpha(1 - M).$$

It then follows from Lemma 2 that $M(t) \leq 1 \forall t > 0$.

Now, for $I > I_c$, (2.16) becomes

$$\begin{aligned} \frac{dM}{dt} &= \frac{kI}{A + \mu(I - I_c)} - \left(\alpha + \frac{\gamma\mu(I - I_c)}{N + \mu(I - I_c)} \right) M \\ &= \frac{kI_c}{A + \mu(I - I_c)} + \frac{k(I - I_c)}{A + \mu(I - I_c)} - \alpha M - \frac{\gamma\mu(I - I_c)}{N + \mu(I - I_c)} M \\ &\leq \frac{kI_c}{A} - \alpha M + \frac{k(I - I_c)}{A + \mu(I - I_c)} - \frac{\gamma\mu(I - I_c)}{N + \mu(I - I_c)} M. \end{aligned} \quad (2.19)$$

Since $\frac{kI_c}{\alpha A} \leq 1$, we have $\frac{kI_c}{A} \leq \alpha$, so (2.19) yields

$$\begin{aligned}
\frac{dM}{dt} &\leq \alpha - \alpha M + \frac{k(I - I_c)}{A + \mu(I - I_c)} \left(1 - \frac{\gamma\mu}{k} \left(\frac{A + \mu(I - I_c)}{N + \mu(I - I_c)} \right) M \right) \\
&= \alpha(1 - M) + \frac{k(I - I_c)}{A + \mu(I - I_c)} (1 - \phi(I - I_c)M) ,
\end{aligned} \tag{2.20}$$

where ϕ is the function defined in Lemma 3. From that result, we know that $\phi(I - I_c) \geq 1 \forall I > I_c$, so $1 - \phi(I - I_c)M \leq 1 - M$. Inequality (2.20) now yields

$$\frac{dM}{dt} \leq \alpha(1 - M) + \frac{k(I - I_c)}{A + \mu(I - I_c)}(1 - M) = \left(\alpha + \frac{k(I - I_c)}{A + \mu(I - I_c)} \right) (1 - M) .$$

So, by Lemma 2, $M(t) \leq M_0 \leq 1 \forall t > 0$.

□

2.4 Parameter Estimation

This model is intended to model human body to evaluate treatment strategies, so it is important to ensure that the parameters are reflective of actual physiological conditions. We embarked on an extensive literature search in order to estimate physiological values for our model parameters. While some of these parameters (e.g. pathogen growth rates) are widely available in the scientific literature, most required creative searching and data manipulation in order to determine a biologically relevant estimate. While the process for finding our parameters varied based upon the ease of quantifying each individual parameter, our general search methodology was as follows:

1. Determine a reasonable biological interpretation of the parameter.
2. Identify quantifiable proxies for the dependent variables associated with the parameter.
3. Identify a “dream data set” relating the proxies from Step 2.
4. Search published models for parameters corresponding to ours, and investigate their values.

(Note: this step is not usually beneficial, but is still worth doing, because, if successful, it can

save a great deal of time.)

5. Search the biological and medical literature for papers containing data matching the “dream data set.” (Note: frequently, this involves synthesizing multiple data sets from multiple sources.)
6. Derive an estimate for the parameter from the given data set.

It would be impractical to present the details of every parameter to which we applied this approach. Instead, we illustrate our method by describing the derivation of our estimates for the parameters μ and I_c from Equation (2.17) (See Section 2.2.3 for the relevant biological details.):

1. μ represents the rate of AIC production per unit of I , the concentration of active immune responders, while I_c is the active immune responder threshold, beyond which the AIC-concentration becomes physiologically relevant.
2. We want data relating $C(I)$ to I . We use IL-10, the most common AIC as our proxy for $C(I)$. We identify I with the concentration of CD14+ cells in the blood. (CD14 serves as a receptor for bacterial antigens and is expressed exclusively on immune responder cells.)
3. Based on the identification in Step 2, one “dream data set” to determine both μ and I_{crit} would be *in vivo* data for IL-10 concentration vs. CD14+-cell concentration.
4. We searched the models described in Section 1.3, but found no parameters that corresponded biologically to μ or I_c .
5. After reviewing many biomedical research papers, we found one by Paats et al ([40]) with measures of IL-6 (a pro-inflammatory mediator) and IL-10 (our anti-inflammatory proxy) versus pneumonia severity index (PSI), a score used to quantify a patient’s 30-day risk of mortality from pneumonia ([17],[16]). We also found work from Louis et al ([31]) which provided data relating TNF- α concentrations to CD14+ cells, which allowed us to convert from pro-inflammatory cytokine measurements to an estimate of I (see Fig. 2.3).

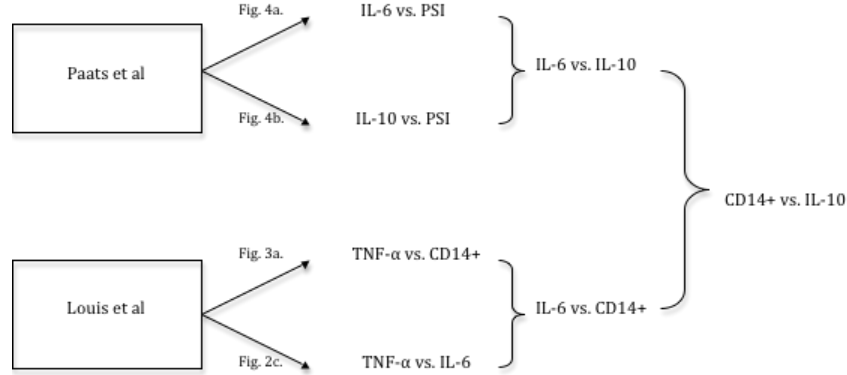


Figure 2.3: Diagram of the process to convert data from Louis et al ([31]) and Paats et al ([40]), in order to estimate a relationship between CD14+, our proxy for I and IL-10, our proxy for $C(I)$.

6. We began by using the Louis et al data to determine a conversion between CD14+ (our proxy for I) and IL-6 (our proxy for $C(I)$). Figure 3a. in the Louis paper plotted TNF- α versus CD14+ and Figure 2c. plotted TNF- α versus IL-6. We fit a line to each of these plots to return an equations for TNF- α as a function of IL-6 and as a function of CD14+. Setting these two equations equal to one another, we determined the following relationship between IL-6 and CD14+:

$$\text{IL-6} = 303 \text{ CD14+} - 42.12. \quad (2.21)$$

Next, we repeated the process for the the Paats data. Figure 4a. from Paats plotted logIL-6 vs. PSI and Figure 4b. plotted logIL-10 vs. PSI. After determining a linear relationship for both data sets, we fit a linear regression to the data, resulting in the following formulas:

$$y_1 = 0.015 * \text{PSI} - 0.694 \quad (2.22)$$

$$y_2 = 0.0148 * \text{PSI} - 0.4408, \quad (2.23)$$

where,

$$y_1 = \log \text{IL-6 and}$$

$$y_2 = \log \text{IL-10.}$$

Solving (2.22) and (2.23) for PSI and setting both sides equal to each other, we get the following relationship:

$$\log \text{IL-10} = 0.9867 * \log \text{IL-6} - 1.1255,$$

and thus,

$$\text{IL-10} = \frac{\text{IL-6}}{10^{1.1255}}.$$

Then, using the formula from (2.21), we get:

$$\text{IL-10} = \frac{303 \text{ CD14+} - 42.12}{10^{1.1255}} = 22.7(\text{CD14+} - 0.139),$$

which becomes for our model:

$$C(I) = 22.7(I - 0.139).$$

This matches the model for $C(I)$ in (2.17), and thus we have $\mu = 22.7$ and $I_c = 0.139$.

Repeating this process for the other model parameters, we were able to generate the estimates shown in Table 2.1, which are used for our numerical experiments in Section 2.5. This was an incredibly time consuming process, and many parameters were simply not quantifiable in the current scientific literature. While we were able to find some biologically relevant estimates, in many cases we simply must estimate our parameters in order to fit the desired final behavior of the system.

2.5 Numerical Experiments

Numerical experiments are a useful tool in demonstrating key properties of our model. In particular, numerical simulations can be used to determine if the model (2.16)-(2.17) maintains the key properties of the Caudill model and to simulate experiments that compare patient outcomes under different treatment protocols. To this end, we determine whether the “immunologic memory” property is retained in our new model, and investigate the incorporation of three different treatment interventions into this model: antibiotics, anti-inflammatory drugs, and infusion with

Table 2.1: Model parameter values used in the numerical demonstrations in Section 2.5.

Parameter	Description (<i>units</i>)	Model Equation	Value	Source
a	Per capita bacterial growth rate (min^{-1})	(2.13)	0.2	[22]
P_{max}	Maximum bacterial concentration (P -cells/ mL)	(2.13)	10^7	[22]
λ	Immunocompetence parameter (<i>unitless</i>)	(2.13), (2.14)	0.8	[4]
b	Bacterial death rate due to immune response (P -cells/ $(I$ -cell \cdot min))	(2.13)	0.0458	[3]
E	Immune kill rate saturation constant (P -cells/ mL)	(2.13)	1.0	estimated
c	Rate of pathogen-induced immune responder activation (P -cells/ $(mL \cdot min)$)	(2.14)	7.0	estimated
K	Pathogen-induced immune activation saturation constant (P -cells/ mL)	(2.14)	100.0	estimated
q	Rate of autocatalysis-induced immune responder activation (I -cells/ $(mL \cdot min)$)	(2.14)	0.6	estimated
B	Autocatalysis-induced immune activation saturation constant (I -cells/ mL)	(2.14)	1.0	estimated
r	Immune responder decay rate (min^{-1})	(2.14)	0.05	[44]
ν	Rate of enhanced immune responder activation due to memory cells (I -cells/ $(Q$ -cell \cdot min))	(2.14)	10.0	estimated
u	Maximum conversion rate of activated immune responders into memory cells (Q -cells/ $(I$ -cell \cdot min))	(2.14), (2.15)	0.5	estimated
χ	Parameter governing conversion rate of activated immune responders ($mL/(P$ -cell))	(2.14), (2.15)	0.5	estimated
κ	Memory cell decay rate (min^{-1})	(2.15)	0.01	estimated

anti-inflammatory cytokines, and the resulting level of tissue damage that follows.

For the purpose of this demonstration, we will focus specifically on bacteria-induced pneumonia, and its impact on respiratory function. Before we can proceed, we must describe precisely what the tissue damage/dysfunction variable M (from model equation (2.16)) represents in this context. The P/F -ratio, defined as the ratio of the partial pressure of arterial oxygen to the fraction of inspired oxygen, is used by a number of lung-function scoring systems, including the widely-used Sequential Organ Failure Assessment (SOFA) score ([56]) and the Lung Injury Score (LIS) ([37]), to quantify lung function. Larger P/F -ratio values indicate greater lung functionality, with values in the 400-500 range being typical for healthy adults [58]. Assuming a maximum P/F -ratio of 500 $mmHg$, we define M in terms of the P/F -ratio like this:

$$M(t) = 1 - \frac{P/Fratio}{500}. \quad (2.24)$$

To provide some context for $M(t)$ in this setting, we list, in Table 2.2, the breakpoints used by LIS

Table 2.2: P/F-ratio (abbreviated PF) ranges used in the lung function subscore of the Lung Injury Score (LIS), with corresponding values for $M(t)$, as defined in Equation (2.24).

LIS Subscore	P/F-ratio Range	$M(t)$ Range
0	$PF > 300$	$M(t) < 0.40$
1	$225 < PF \leq 300$	$0.40 \leq M(t) < 0.55$
2	$175 < PF \leq 225$	$0.55 \leq M(t) < 0.65$
3	$100 < PF \leq 175$	$0.65 \leq M(t) < 0.80$
4	$PF \leq 100$	$M(t) \geq 0.80$

to distinguish different levels of lung dysfunction, and the corresponding $M(t)$ -values.

2.5.1 Memory Property Experiment

First, we demonstrate that the model (2.13)-(2.15) retains the immunologic memory property, by determining the state of two patients who differ only in previous exposure to the causative pathogen. In this model, prior exposure to a pathogen in a host would be indicated by a positive Q_0 -value. Using the parameters from Table 2.1, an initial pathogen load P_0 of 100 P -cells/mL and an initial active immune responder load of 0, we ran experiments in two hosts. The “immunologic memory” host had an initial memory cell concentration (Q_0) of 200 Q -cells/mL, while the “no memory” host had $Q_0 = 0$.

The results from this experiment are shown in Figure 2.4. The “immunologic memory” host is able to clear the pathogen threat (plot (a)) while the otherwise identical “no memory” host’s immune system is overwhelmed by the pathogen (plot (b)). The presence of memory immune cells in the “immunologic memory” host allows the active immune responder population to rapidly increase, creating a strong defense against the pathogen (plot (c)), while the “no-memory” host takes a longer time to build an immune response (plot (d)), and is subsequently unable to combat

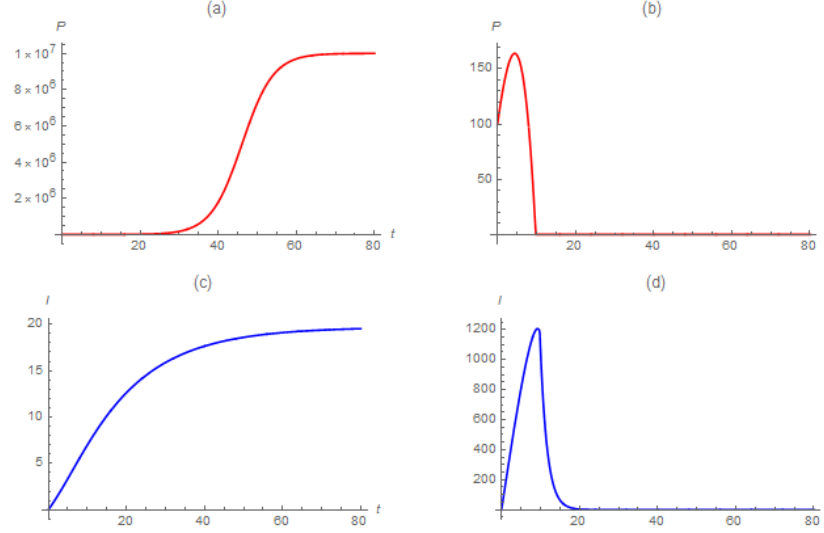


Figure 2.4: Results of immunological memory property demonstration: (a) Plot of pathogen concentration vs. time for “immunologic memory” property host, (b) plot of pathogen concentration vs. time for “no memory” host, (c) plot of active immune responder concentration vs. time for “immunologic memory” property host, (d) plot of active immune responder concentration vs. time for “no memory” host.

the pathogen threat (plot (b)). Therefore, we confirm that the “immunologic memory” property is maintained in the updated model (2.13)-(2.15).

2.5.2 Antibiotic treatment

Following [5, 6], we incorporate the pathogen-killing effect of an antibiotic by augmenting (2.13) with an additional removal term of the form

$$d(A - \Lambda)P,$$

where $A = A(t)$ gives the concentration of the antibiotic in the blood at time t , and the function $d(A - \Lambda)$ is defined as

$$d(A - \Lambda) = \begin{cases} 0 & \text{if } A - \Lambda \leq 0 \\ \frac{v(A - \Lambda)}{1 + w(A - \Lambda)} & \text{if } A - \Lambda > 0 \end{cases}. \quad (2.25)$$

The constant Λ in (2.27) is the *minimum inhibitory concentration (MIC)* of the antibiotic with respect to the pathogen. The MIC represents the minimum antibiotic concentration required to prevent the pathogen population from growing, and is a standard measure of the level of susceptibility of the pathogen to that antibiotic. The constants v and w in (2.25) are characteristics of the pathogen-antibiotic combination. Note that the piecewise structure of (2.25) results in the antibiotic having no killing effect unless the antibiotic concentration A exceeds the MIC Λ .

We model the time-evolution of the antibiotic concentration A via standard pharmacokinetics models. (See, e.g., [19].), as follows: For a single dose of G mg of a drug administered via bolus injection (i.e. injected instantaneously directly into the bloodstream) at time t_0 , the amount $A^{(1)}(t)$ of this dose that remains in the bloodstream at any later time t may be approximated by

$$A^{(1)}(t) = Ge^{-h(t-t_0)}, \quad t \geq t_0,$$

for some positive constant h . If additional doses of the same amount G are given, each T hours after the preceding one, then the amount of the j th dose (given at time $t_0 + (j-1)T$) that remains at a later time t will be

$$A^{(j)}(t) = Ge^{-h(t-(t_0+(j-1)T))}, \quad t \geq t_0 + (j-1)T. \quad (2.26)$$

Noting that the total concentration $A(t)$ of drug in the bloodstream at time t is the sum of the amounts remaining from all previous doses, divided by the patient's blood volume V , we have the model

$$A(t) = \begin{cases} 0 & \text{if } t < t_0 \\ \frac{1}{V} \sum_{j=1}^{\lceil \frac{t-t_0}{T} \rceil} A^{(j)}(t) & \text{if } t_0 \leq t < t_0 + (J-1)T \\ \frac{1}{V} \sum_{j=1}^J A^{(j)}(t) & \text{if } t \geq t_0 + (J-1)T \end{cases}, \quad (2.27)$$

where J is the total number of doses given, and the square brackets represent the ceiling function

(i.e. the smallest integer that is not less than the argument inside the brackets). So, we incorporate antibiotic usage into our tissue damage model (2.13)-(2.17) by replacing (2.13) with

$$\frac{dP}{dt} = \frac{aP}{\lambda} \left(1 - \frac{P}{P_{max}}\right) - \frac{bPI}{\lambda(E+P)} - d(A - \Lambda)P, \quad P(0) = P_0, \quad (2.28)$$

and incorporating equation (2.27). The antibiotic-kill term is additive – if the patient is being treated with, say, two different antibiotics, then the removal term $-d(A - \Lambda)P$ is replaced by a pair of terms $-d_1(A_1 - \Lambda_1)P - d_2(A_2 - \Lambda_2)P$, where A_j , Λ_j , and d_j correspond to antibiotic j . (The functions d_1 and d_2 both correspond to equation (2.25), but with different parameter values.)

2.5.3 Use of anti-inflammatory drugs

When inflammation leads to tissue and organ damage or dysfunction, a patient may be given one or more medications intended to reduce inflammation to less-destructive levels. Here, we focus on *non-steroidal anti-inflammatory drugs (NSAIDs)* like ibuprofen, aspirin, and naproxin. Assuming that the drug is administered in the same fashion (multiple equal doses given at fixed time intervals) as the antibiotic in the previous subsection, and assuming that this NSAID follows the same pharmacokinetics as the antibiotic, then we can use equation (2.27) (suitably re-labeled) to model the NSAID concentration $D(t)$ over time. We model the effects of the NSAID as a reduction in the population size of the activated immune responders I . So, we incorporate NSAID usage into our tissue damage model (2.13)-(2.17) by replacing (2.14) with

$$\frac{dI}{dt} = \sqrt{\lambda} \left(c + \nu Q + \frac{qI}{B+I} \right) \frac{P}{K+P} - \frac{rI}{\lambda} - uIe^{-\chi P} - \frac{pDI}{L+D}, \quad I(0) = I_0, \quad (2.29)$$

where

$$g(D) = \frac{1}{V} \left(1 - \frac{D}{U+D} \right), \quad (2.30)$$

and adding equation (2.27) with $A(t)$ replaced by $D(t)$.

2.5.4 Infusion with anti-inflammatory cytokines

Within the past two decades, researchers have investigated the use of anti-inflammatory cytokines (AIC) (principally Interleukin-10, or IL-10) as therapeutic agents for inflammation-based health challenges, including psoriasis ([43]), inflammatory bowel disease ([30]), and Crohn's disease ([48]). IL-10 has also been investigated as a means to mediate the negative impact of excessive inflammation consequent to viral (e.g. hepatitis C [38]) and bacterial (e.g. *Pseudomonas aeruginosa* pneumonia [51]) infections. Here, we will model AIC therapy as a series of instantaneous infusions of AIC that raise the bloodstream concentration of AIC from $C(I)$ to $C(I) + \Gamma(t)$. Assuming multiple administrations of the same dosage at fixed time intervals, and assuming first-order removal kinetics, we can model the time-evolution of $\Gamma(t)$, representing the additional AIC concentration due to this therapy, with equation (2.27) with $A(t)$ replaced by $\Gamma(t)$. Then, we incorporate AIC therapy into our tissue damage model (2.13)-(2.17) by replacing (2.16) with

$$\frac{dM}{dt} = \frac{kI}{1 + \rho(C(I) + \Gamma(t))} - \left(\alpha + \frac{\gamma(C(I) + \Gamma(t))}{N + (C(I) + \Gamma(t))} \right) M, \quad M(0) = M_0, \quad (2.31)$$

and adding equation (2.27) with $A(t)$ replaced by $\Gamma(t)$.

2.5.5 Treatment Experiments

Efforts to minimize the rise and spread of antibiotic-resistant (AR) bacterial pathogens have focused, in large part, on the use of broad-spectrum antibiotics, i.e. drugs that are effective against a wide-range of bacterial species. Broad-spectrum agents are often used as front-line therapy for suspected bacterial infections, because the causative agent is rarely known at the time treatment is initiated. The frequent exposure of pathogen populations to these antibiotics increases the likelihood that genetic mutations, with decreased susceptibility to the antibiotic, will grow to dominate the pathogen population. To combat this, hospitals often recommend, as an antibiotic stewardship measure, for clinicians to culture an infection immediately after initial diagnosis, to identify the causative pathogen species. Once the pathogen is identified, the broad-spectrum antibiotic treatment is discontinued, in favor of treatment with a narrow-spectrum antibiotic that

specifically targets this particular pathogen, with the intention of minimizing the total volume of broad-spectrum antibiotic used hospital-wide.

In recent years, researchers have proposed an alternative protocol that eliminates the use of broad-spectrum antibiotics during the period from initial diagnosis to pathogen identification, in favor of anti-virulence drugs during this initial treatment period [8, 42]. The idea is to minimize the negative impact of the pathogen's presence during the initial treatment period, to buy time for two things to happen: (i) pathogen identification results to become available, and (ii) the patient's immune response to activate against the infection [54]. Anti-virulence agents may work by interfering directly with vital bacterial functions ([20, 42, 60]), counteracting the effects of bacterial toxins ([15, 24, 47]), or ameliorating the destructive effects of the pro-inflammatory immune response ([51]).

To demonstrate the potential of our model in clinical investigation, we will use it to simulate an experiment in which three patients, identical in all relevant ways and facing the same bacterial pneumonia challenge, receive three different forms of initial therapy during the first 24 hours of treatment:

- Patient 1 is treated with the broad-spectrum antibiotic imipenem for the first 24 hours.
- Patient 2 is treated with an NSAID for the first 24 hours.
- Patient 3 is treated with AIC infusion for the first 24 hours.

At the 24-hour mark, we assume that the causative pathogen has been identified, and the initial therapies for all four patients are replaced by treatment with the narrow-spectrum antibiotic oxacillin.

Studies suggest that P/F-ratio alone, as a measure of hypoxemia, is not a good predictor of patient outcome in pneumonia, but that a combination of hypoxemia severity and time-duration of that severity serves as a more effective predictor [35, 59]. Consequently, we will use the quantity

$$M_{24}(t) \equiv \frac{1}{24} \int_{t-24}^t M(s) ds, \quad t \geq 24,$$

Table 2.3: Model parameter values used in the numerical HAP experiment in Section 2.5.

Parameter	Description (<i>units</i>)	Model Equation	Value	Source
k	Rate of development of tissue damage/dysfunction due to immune response ($(M\text{-cells} \cdot pg)/(I\text{-cell} \cdot mL \cdot min)$)	(2.16)	2.14	estimated
A	Saturation constant for immune-induced tissue damage (pg/mL)	(2.16)	6.0	estimated
α	Baseline rate of tissue repair/recovery (min^{-1})	(2.16)	0.05	[44]
γ	Tissue repair/recovery rate enhancement due to anti-inflammatory cytokine activity (min^{-1})	(2.16)	0.1	estimated
N	Saturation constant for tissue repair/recovery enhancement (pg/mL)	(2.16)	1.0	estimated
μ	Per capita anti-inflammatory cytokine rate of production by activated immune responders ($pg/(I\text{-cell})$)	(2.16), (2.17)	22.7	[31, 40]
δ_I	Half-width of transition I -interval for $C(I)$ ($I\text{-cells}/mL$)	(2.17)	0.05	
I_c	Immune responder concentration corresponding to a critical concentration of anti-inflammatory cytokines ($I\text{-cells}/mL$)	(2.17)	0.139	[31, 40]
V	Blood volume of patient (L)	(2.27)	5.5	

representing a rolling 24-hour average of respiratory damage/dysfunction, as our outcome of interest for each patient. We simulate each patient’s progress over a 96-hour period with the model parameter values listed in Tables 2.1 and 2.3, and the treatment parameter values listed in Table 3.1. Each patient begins with $P_0 = 10^4$ and $I_0 = Q_0 = M_0 = 0$.

Numerical implementation of our tissue damage model, and its variants, requires special handling in the event of small pathogen population size. In this setting, our representation of this population by a continuous quantity diverges from reality in the following sense: In reality, complete pathogen clearance is possible in finite time, whereas, this is not possible in our model system. (The validity of the “continuous pathogen population” assumption is a decreasing function of pathogen population size.) As a result, a positive initial pathogen population will remain forever positive (although infinitesimally small, in the case of effective treatment) within our system. Consequently, when the immune response returns to its pre-challenge state and when treatments have ceased, the infinitesimally-small pathogen population will grow, eventually to levels that again trigger an immune response, and, possibly, additional tissue damage. Left unaddressed, this cycle will continue

Table 2.4: User-defined treatment-specific model parameter values used in the numerical HAP experiment in Section 2.5.5. Abbreviations in the table: BS-AB = broad-spectrum antibiotic (imipenem), NS-AB = narrow-spectrum antibiotic (oxacillin), NSAID = non-steroidal anti-inflammatory drug, AIC = anti-inflammatory cytokine.

Parameter	Description (<i>units</i>)	Model Equation	BS-AB	NS-AB	NSAID	AIC
G	Dosage (mg)	(2.26)	500	2000	800	600
h	Decay rate parameter (hr^{-1})	(2.26)	0.12	0.12	0.35	0.082
T	Time between consecutive doses (hr)	(2.27)	4	6	6	8
Λ	MIC of pathogen ($\mu g/mL$)	(2.25)	1.0	4.0	—	—
v	AB-induced kill-rate parameter (min^{-1})	(2.25)	0.5	0.6	—	—
w	AB-induced kill-rate parameter ($\mu g/mL$)	(2.25)	1.0	1.0	—	—
U	Saturation constant in NSAID effect ($\mu g/mL$)	(2.30)	—	—	12.0	—

in the model system indefinitely. We manage this issue by introducing a thresholding criterion into our numerical implementation. Specifically, we set a threshold for the pathogen population, and agree to consider any population size below the threshold as equivalent to zero. Implementation involves stopping the ODE integration periodically, and comparing the current pathogen population size to the threshold value, resetting the former to zero if it is smaller than the latter. For the experimental results here, we use a threshold of 10^{-4} cells/mL, applied every 9.6 hours.

Numerical results over the first 96 hours of treatment are shown in Figures 2.5 and 2.6. Figure 2.5 shows $M(t)$ vs. time for each patient, reflecting the time-course of lung function recovery. All four patients have comparable peak levels of lung dysfunction, but recover at different rates. As expected, Patient 1 (broad-spectrum antibiotic initially) recovers lung function most quickly, while Patient 4 (no treatment initially) takes the longest to recover. Of the remaining two, Patient 3 (AIC infusion initially) fares better than Patient 2 (NSAID initially) for a while, although their $M(t)$ -profiles are comparable beyond 72 hours, as the transient effects of the initial treatments are essentially gone. Figure 2.6 shows $M_{24}(t)$ vs. time for each patient, reflecting risk of death or other complicating event. For each patient, the peak M_{24} -value exceeds 0.55, indicating a moderate-level of lung dysfunction. However, the length of time at which this threshold is exceeded varies between patients, with Patient 1 the smallest, followed by Patients 3, 2, and 4.

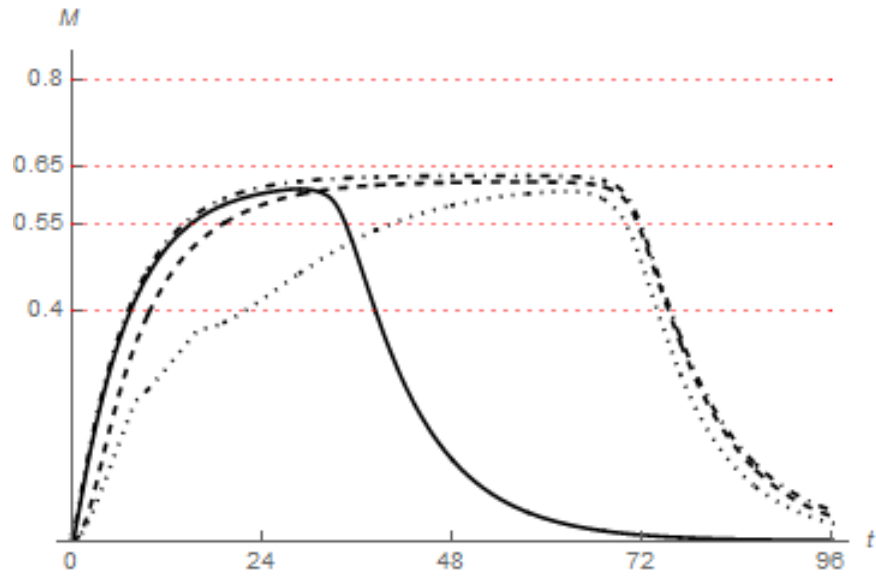


Figure 2.5: Tissue damage measure $M(t)$ vs. time (t , in hours) for the four patients in the numerical experiment: Solid = Patient 1, dashed = Patient 2, dotted = Patient 3, and dot-dashed = Patient 4. Horizontal lines represent LIS breakpoints from Table 2.2.

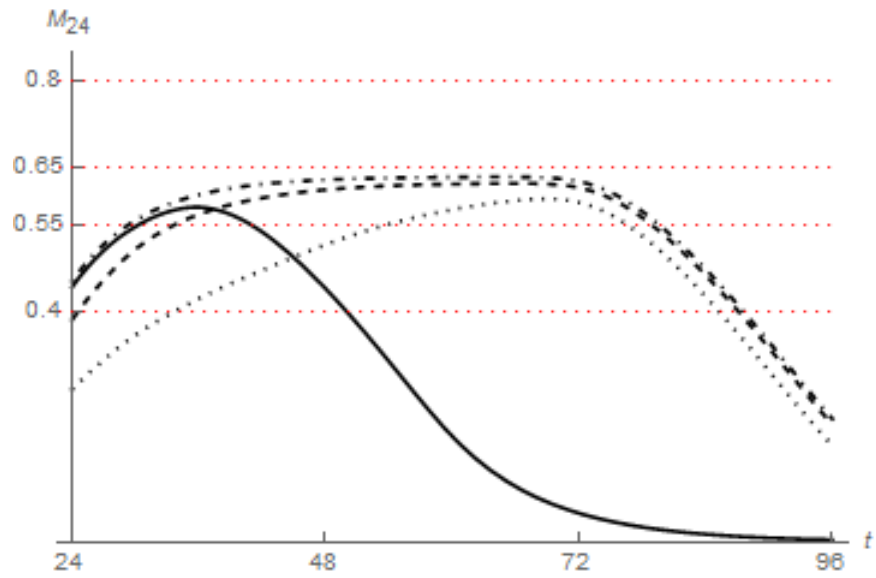


Figure 2.6: Moving 24-hour average M_{24} of tissue damage measure $M(t)$ vs. time (t , in hours) for the four patients in the numerical experiment: Solid = Patient 1, dashed = Patient 2, dotted = Patient 3, and dot-dashed = Patient 4. Horizontal lines represent LIS breakpoints from Table 2.2.

Given the number of model parameters that were estimated by the authors, we must be clear that these simulation results do not imply any comparative advantages for AIC-infusion over NSAID treatment as alternatives for initial broad-spectrum antibiotic use. Rather, this work should be understood as an illustration of the types of controlled experiments that may be simulated with the present model, given biologically realistic parameter values.

Chapter 3

Multiple Organ Damage Model

3.1 Biological Background

Like most things, organ failure does not occur in a vacuum. Each organ system is interdependent on the others, and impaired function in one organ can result in widespread damage throughout the entire body. Even if an infection is localized to one specific organ, the damage inflicted to that organ can have significant downstream effects in other organ systems. For example, the lungs are responsible for re-oxygenating the body's bloodstream, and thus control the oxygen supply to all tissues and organs. The kidneys, which filter waste from the bloodstream, are critically important in maintaining healthy organ function. Furthermore, the kidneys require a consistent oxygen source in order to properly function [21], so lung dysfunction can lead to kidney dysfunction. Conversely, damage in the kidney releases excess toxins into the bloodstream, causing inflammation in the lungs, indicating a critical feedback dynamic between the two organ systems. Our goal is to extend our model to include this feedback between lungs and kidneys, which will allow us to investigate the effect of antibiotic use on kidney function. The CDC reports that two of the three most common HAIs include ventilator-associated pneumonia and catheter-associated urinary tract infections [18], so building our model between these two organ systems is consistent with our overall goal of studying antibiotic resistance in a hospital setting.

3.1.1 Effect of Hypoxemia on Kidneys

Impaired lung function can result in hypoxemia, a state of low blood oxygen, which causes hypoxia, in which organ tissues become deprived of oxygen [33]. Hypoxemia has widespread effects throughout the body, including respiratory acidosis, right-sided heart failure, cyanosis, tachycardia, and edema [33]. In the kidneys, hypoxemia has been shown to cause decreased renal output, decreased glomerular filtration rate (GFR), and acute tubular necrosis (a condition characterized by the rapid death of tubule cells, which help transport waste through the kidney) ([33], [50], [10], [2]).

The primary function of the kidneys is to filter waste from the bloodstream. Thus, when this ability is compromised, the repercussions can be devastating. Kidney function can be measured clinically in a number of ways. Creatinine, a byproduct of the breakdown of creatine phosphate during muscle metabolism, is produced by the body at a constant rate. Thus, when kidney function is impaired, the concentrations of creatinine in the bloodstream or in urine will be elevated, indicating a problem. GFR measures the rate at which waste (e.g. creatinine, urea) flows through the kidneys. A low GFR indicates dysfunction, and a possible build up of toxins in the kidneys.

3.1.2 Effect of Kidney Damage on Lungs

Evidence suggests that, when respiratory failure and acute kidney injury (AKI) occur together, the chance of survival is only 20%, principally because impaired lung function impacts kidney function, and that subsequent kidney damage can also result in further damage to the lungs [14]. By limiting their ability to filter waste, damage to the kidneys results in increased serum creatinine and urea [33]. This can result in severe damage to multiple organ systems, including the lung [33]. In high concentrations, creatinine in the lungs can activate the pro-inflammatory immune response, resulting in further lung damage [27].

3.2 Proposed Model

Our mathematical model of inflammation-induced tissue damage builds on our single organ damage model and incorporates the effects of hypoxemia and increased serum creatinine on kidney and organ

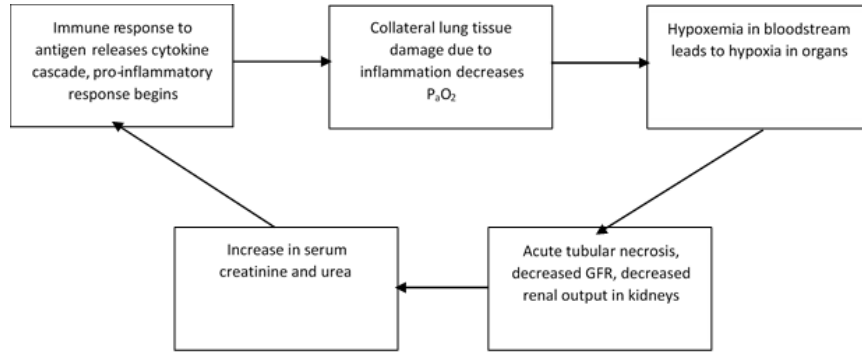


Figure 3.1: A schematic diagram between the damage and feedback dynamics of inflammatory lung and kidney damage.

function. Though our model currently simulates a two-organ system, we allow for the possibility to incorporate additional organs and their dynamics.

We describe the development of our multi-organ damage model in two parts: first, we copy our single-organ pathogen-induced damage model and localize it to either organ system (the lungs or the kidneys). Second, we link the two organ systems through creatinine and arterial oxygen.

We base our two-organ model upon the single-organ model described in Section 2.2. Since the dynamics of pathogen-induced inflammation described in our single-organ damage model are not limited to one particular organ, and to allow for the possibility of an infection originating in either organ, we simply duplicate our 4x4 ODE model. We affix the subscripts “L” to variables that apply to the lung and “K” for variables that apply to the kidney:

$$\frac{dP_L}{dt} = \frac{a_L P_L}{\lambda} \left(1 - \frac{P_L}{P_{L,max}}\right) - \frac{b_L P_L I_L}{\lambda(E_L + P_L)}, \quad P_L(0) = P_{L,0}, \quad (3.1)$$

$$\frac{dI_L}{dt} = \sqrt{\lambda} \left(c_L + \nu_L Q_L + \frac{q_L I_L}{B_L + I_L}\right) \frac{P_L}{K_L + P_L} - \frac{r_L I_L}{\lambda} - u_L I_L e^{-\chi_L P_L}, \quad I_L(0) = I_{L,0}, \quad (3.2)$$

$$\frac{dQ_L}{dt} = u_L I_L e^{-\chi_L P_L} - \kappa_L Q_L, \quad Q_L(0) = Q_{L,0}, \quad (3.3)$$

$$\frac{dM_L}{dt} = \frac{k_L I_L}{A_L + G_L(I_L)} - \left(\alpha_L + \frac{\gamma_L G_L(I_L)}{N_L + G_L(I_L)}\right) M_L, \quad M_L(0) = M_{L,0}, \quad (3.4)$$

$$\frac{dP_K}{dt} = \frac{a_K P_K}{\lambda} \left(1 - \frac{P_K}{P_{K,max}}\right) - \frac{b_K P_K I_K}{\lambda(E_K + P_K)}, \quad P_K(0) = P_{K,0}, \quad (3.5)$$

$$\frac{dI_K}{dt} = \sqrt{\lambda} \left(c_K + \nu_K Q_K + \frac{q_K I_K}{B_K + I_K}\right) \frac{P_K}{K_K + P_K} - \frac{r_K I_K}{\lambda} - u_K I_K e^{-\chi_K P_K}, \quad I_K(0) = I_{K,0} \quad (3.6)$$

$$\frac{dQ_K}{dt} = u_K I_K e^{-\chi_K P_K} - \kappa_K Q_K, \quad Q_K(0) = Q_{K,0}, \quad (3.7)$$

$$\frac{dM_K}{dt} = \frac{k_K I_K}{A_K + G_K(I_K)} - \left(\alpha_K + \frac{\gamma_K G_K(I_K)}{N_K + G_K(I_K)}\right) M_K, \quad M_K(0) = M_{K,0}, \quad (3.8)$$

where, for $X = L$ or $X = K$,

$$C_X(I) = \begin{cases} 0 & \text{if } I_X \leq I_{X,c} - \delta_{X,I} \\ \frac{\mu}{4\delta_{X,I}} (I_X - (I_{X,c} - \delta_{X,I}))^2 & \text{if } I_{X,c} - \delta_{X,I} < I_X \leq I_{X,c} + \delta_{X,I} \\ \mu(I_X - I_{X,c}) & \text{if } I_X > I_{X,c} + \delta_{X,I} \end{cases} \quad (3.9)$$

Next, we turn to modeling the linkage between the lungs and kidneys through arterial oxygen and creatinine.

3.2.1 Modeling Blood Oxygen

The mechanism of kidney damage due to hypoxemia, as described in Section 3.1 and Fig. 3.1, is due to decreased arterial oxygen pressure, so we must model the oxygen-level of the blood flowing to the kidneys. Since the kidneys receive their blood directly from the lungs through the renal artery,

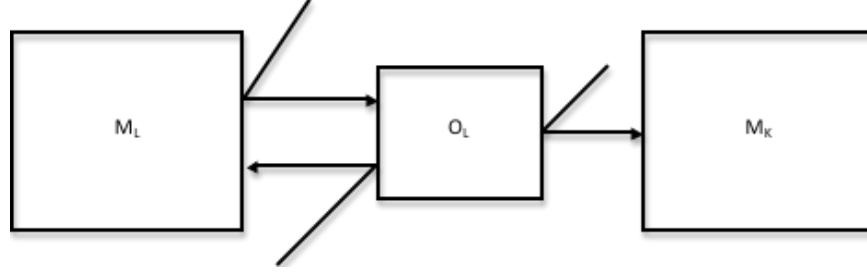


Figure 3.2: Box model of the process of lung-kidney dysfunction due to decreased oxygen levels.

we assume that the partial pressure of the blood leaving the lungs, which we denote O_L , is the same as the partial pressure of the blood entering the kidneys. Since, as described in Section 2.5, we quantify lung function by the PF-ratio, we incorporate the F_iO_2 (fraction of inspired oxygen) value O_{insp} . This will also allow us to investigate the effects of mechanical ventilation, which often provides patients with an inspired oxygen level higher than atmospheric oxygen.

We derive our function for arterial oxygen pressure by starting with the PF-ratio formula:

$$PF = \frac{P_aO_2}{F_iO_2} = \frac{O_L}{O_{insp}}.$$

Then, since a patient's PF-score decreases with lung function, we know that a patient's PF-score for a given level of functionality is a decreasing function of M_L , with some maximum healthy PF-score (which we denote $O_{L,healthy}$), or:

$$PF = O_{L,healthy}(1 - M_L),$$

so:

$$O_{L,healthy}(1 - M_L) = \frac{O_L}{O_{insp}}.$$

Rearranging to solve for O_L gives us:

$$O_L = O_{L,healthy}(1 - M_L)O_{insp}, \tag{3.10}$$

which expresses O_L as an explicit function of lung dysfunction, M_L .

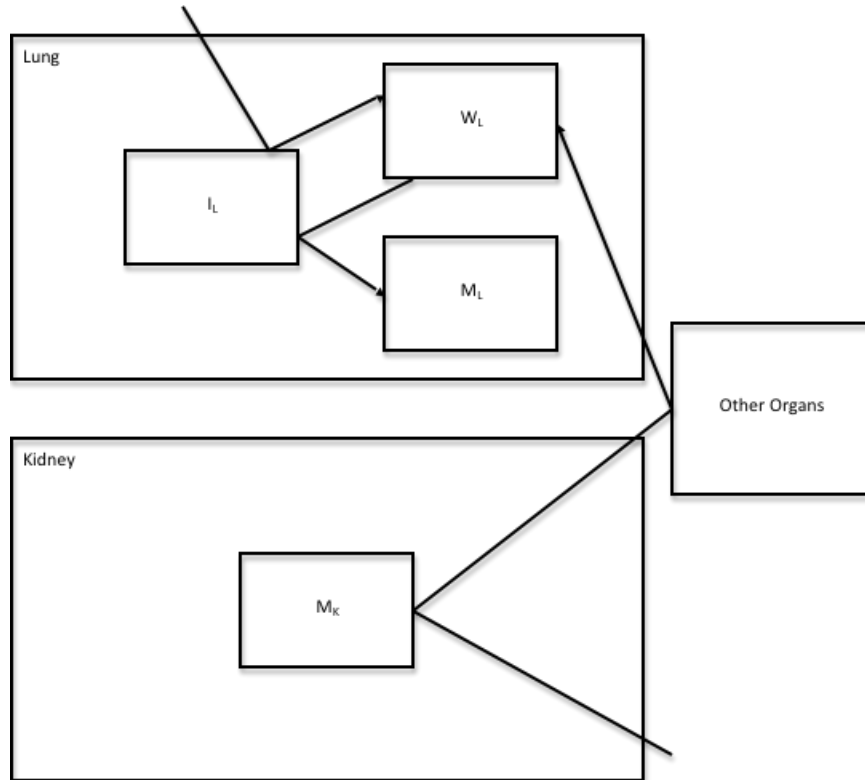


Figure 3.3: Box model of the process of lung-kidney dysfunction due to increased serum creatinine.

3.2.2 Modeling Creatinine Levels

Since kidney function is measured by the rate of filtration of creatinine and other waste products, we must incorporate a measure of creatinine levels in the bloodstream. Since increased serum creatinine levels cause damage by activating the immune response in the lung, we must incorporate a term for lung creatine, W_L . Because the elevated creatinine in the body is a result of impaired kidney function, the additional concentration of creatinine in the lung is dependent on kidney dysfunction, M_K . However, we must also account for the time it takes for the creatinine-filled blood to flow from the kidneys and settle in the lungs by incorporating the time that it takes for blood to cycle through the organs and return to the lungs, which we denote Δt .

Assuming an initial concentration of creatinine $W_{L,0}$ at time $t = 0$, we model the rate of creatinine clearance with an exponential decay term, with removal dependent on the presence of active immune responders, I_L .

$$\frac{dW_L}{dt} = -\psi I_L W_L, \quad W_L(n\Delta t) = W_{L,n\Delta t}, \quad (3.11)$$

where

$$W_L(0) = W_{L,0}, \quad (3.12)$$

$$W_{L,n\Delta t} = \max [R + \rho W_L((n-1)\Delta t) - W_{max}(M_K((n-1)\Delta t)), 0], \quad (3.13)$$

$$W_{max}(M_K) = C_{max,0}(1 - M_K). \quad (3.14)$$

The initial value for the creatinine concentration is recalculated for every Δt time step of the model, starting at time $t = 0$, based upon the concentration of creatinine in the lungs and the level of kidney dysfunction one blood cycle earlier. $W_{max}(M_K)$ is a decreasing function of M_K and represents the maximum concentration of creatinine that the kidney can process for a given level of kidney damage. If the creatinine level output from the lungs from the previous blood cycle (denoted by the term $\rho W_L((n-1)\Delta t)$) plus the creatinine output from the auxiliary organs (a constant, R) is greater than the $W_{max}(M_K)$ value for M_K during the $(n-1)^{st}$ blood cycle, then that excess concentration will be deposited in the lungs, becoming the starting lung creatinine concentration for the n^{th} blood cycle. Otherwise, the initial creatinine level in the lung will simply be 0.

3.2.3 Consequences of Oxygen- and Creatinine-Levels

Next, we model the impact of O_L on kidney function, and of W_L on lung function. While we have shown that hypoxia can cause significant lung damage, elevated oxygen levels (known as *hyperoxia*) can have negative consequences as well. As demonstrated in ([32]), hyperoxia leads to the release of reactive oxygen species, which cause damage to healthy tissues. Therefore, we incorporate an additional damage term $f_L(O_L)$ to (3.4) that propagates lung tissue damage when blood-oxygen levels are either above or below the healthy level, $O_{L,healthy}$:

$$f_L(O_L) = \omega(O_L - O_{L,healthy})^2.$$

Then, model equation 2.16 becomes,

$$\frac{dM_L}{dt} = \frac{k_L I_L}{A_L + C_L(I_L)} - \left(\alpha_L + \frac{\gamma_L C_L(I_L)}{N_L + C_L(I_L)} \right) M_L + f_L(O_L) \quad (3.15)$$

$$= \frac{k_L I_L}{A_L + C_L(I_L)} - \left(\alpha_L + \frac{\gamma_L C_L(I_L)}{N_L + C_L(I_L)} \right) M_L + \omega(O_L - O_{L,healthy})^2. \quad (3.16)$$

As noted in Sec. 3.1.2, the presence of circulating creatinine and urea in the bloodstream causes an inflammatory response in the lungs. Thus, we will treat W_L , the creatinine level in the lung, as an immune-provoking toxin, using the model structure of Alex and Painter [1]. Specifically, we add a W_L -dependent term $g(W_L)$ to the lung immune responder equation (3.2):

$$g(W_L) = \frac{\eta W_L}{H + W_L}$$

Then, model equation (3.2) becomes,

$$\frac{dI_L}{dt} = \sqrt{\lambda} \left(c_L + \nu_L Q_L + \frac{q_L I_L}{B_L + I_L} \right) \frac{P_L}{K_L + P_L} - \frac{r_L I_L}{\lambda} - u_L I_L e^{-\chi_L P_L} + g(W_L) \quad (3.17)$$

$$= \sqrt{\lambda} \left(c_L + \nu_L Q_L + \frac{q_L I_L}{B_L + I_L} \right) \frac{P_L}{K_L + P_L} - \frac{r_L I_L}{\lambda} - u_L I_L e^{-\chi_L P_L} + \frac{\eta W_L}{H + W_L}. \quad (3.18)$$

We model the additional damage to the kidney due to reduced blood oxygen levels (O_L) as an additional term $f_K(O_L)$ for the kidney dysfunction equation (3.8). Since we use GFR as our biological indicator of kidney damage, we can assume that kidney dysfunction, M_K , is a decreasing function of GFR. In the absence of pathogen-induced inflammation, we represent this relationship by

$$M_K = 1 - \frac{GFR}{GFR_{healthy}},$$

so by the Chain Rule,

$$\frac{dM_K}{dt} = f_K(O_L) = -\frac{1}{GFR_{healthy}} \frac{dGFR}{dt}.$$

Since $\frac{dGFR}{dt}$ is proportional to the difference between the blood oxygen level and the healthy

$(O_{L,healthy} - O_L)$, this becomes:

$$f_K(O_L) = \phi(O_L - O_{L,healthy}),$$

where $\phi \propto \frac{1}{GFR_{healthy}}$. Adding this term to model equation (3.8) to account for the possibility of inflammation-induced damage, we get:

$$\frac{dM_k}{dt} = \frac{k_K I_K}{A_K + C_K(I_K)} - \left(\alpha_K + \frac{\gamma_K C_K(I_K)}{N_K + C_K(I_K)} \right) M_K + f_K(O_L) \quad (3.19)$$

$$= \frac{k_K I_K}{A_K + C_K(I_K)} - \left(\alpha_K + \frac{\gamma_K C_K(I_K)}{N_K + C_K(I_K)} \right) M_K + \phi(O_L - O_{L,healthy}). \quad (3.20)$$

3.2.4 Final Model

Incorporating equations (3.10) - (3.19) into the model described by equations (3.1) - (3.9) results in the following final model:

$$\frac{dP_L}{dt} = \frac{a_L P_L}{\lambda} \left(1 - \frac{P_L}{P_{L,max}}\right) - \frac{b_L P_L I_L}{\lambda(E_L + P_L)}, \quad P_L(0) = P_{L,0}, \quad (3.21)$$

$$\frac{dI_L}{dt} = \sqrt{\lambda} \left(c_L + \nu_L Q_L + \frac{q_L I_L}{B_L + I_L} \right) \frac{P_L}{K_L + P_L} - \frac{r_L I_L}{\lambda} - u_L I_L e^{-\chi_L P_L} + \frac{\eta W_L}{H + W_L}, \quad I_L(0) = I_{L,0}, \quad (3.22)$$

$$\frac{dQ_L}{dt} = u_L I_L e^{-\chi_L P_L} - \kappa_L Q_L, \quad Q_L(0) = Q_{L,0}, \quad (3.23)$$

$$\frac{dM_L}{dt} = \frac{k_L I_L}{A_L + C_L(I_L)} - \left(\alpha + \frac{\gamma_L C_L(I_L)}{N_L + C_L(I_L)} \right) M_L + \omega(O_L - O_{L,healthy})^2, \quad M_L(0) = M_{L,0}, \quad (3.24)$$

$$\frac{dP_K}{dt} = \frac{a_K P_K}{\lambda} \left(1 - \frac{P_K}{P_{K,max}}\right) - \frac{b_K P_K I_K}{\lambda(E_K + P_K)}, \quad P_K(0) = P_{K,0}, \quad (3.25)$$

$$\frac{dI_K}{dt} = \sqrt{\lambda} \left(c_K + \nu_K Q_K + \frac{q_K I_K}{B_K + I_K} \right) \frac{P_K}{K_K + P_K} - \frac{r_K I_K}{\lambda} - u_K I_K e^{-\chi_K P_K}, \quad I_K(0) = I_{K,0} \quad (3.26)$$

$$\frac{dQ_K}{dt} = u_K I_K e^{-\chi_K P_K} - \kappa_K Q_K, \quad Q_K(0) = Q_{K,0}, \quad (3.27)$$

$$\frac{dM_K}{dt} = \frac{k_K I_K}{A_K + C_K(I_K)} - \left(\alpha_K + \frac{\gamma_K C_K(I_K)}{N_K + C_K(I_K)} \right) M_K + \phi(O_L - O_{L,healthy}), \quad M_K(0) = M_{K,0}, \quad (3.28)$$

$$O_L = O_{L,healthy}(1 - M_L)O_{insp} \quad (3.29)$$

$$\frac{dW_L}{dt} = -\psi I_L W_L, \quad W_L(n\Delta t) = W_{L,n\Delta t}, \text{ where,} \quad (3.30)$$

$$W_{L,n\Delta t} = \max[R + \rho W_L((n-1)\Delta t) - W_{max}(M_K((n-1)\Delta t)), 0] \text{ and } W_L(0) = W_{L,0}, \quad (3.31)$$

$$W_{max}(M_K) = W_{max,0}(1 - M_K) \quad (3.32)$$

where, for $X = L$ or $X = K$,

$$C_X(I_X) = \begin{cases} 0 & \text{if } I_X \leq I_{X,c} - \delta_{X,I} \\ \frac{\mu}{4\delta_{X,I}} (I_X - (I_{X,c} - \delta_{X,I}))^2 & \text{if } I_{X,c} - \delta_{X,I} < I_X \leq I_{X,c} + \delta_{X,I} \\ \mu(I_X - I_{X,c}) & \text{if } I_X > I_{X,c} + \delta_{X,I} \end{cases} \cdot \quad (3.33)$$

3.3 Numerical Experiments

The model (3.21)-(3.33) can provide a number of interesting insights into the dynamics of cascading lung-kidney damage. In particular, it can validate results observed in a clinical setting. Since our experiments in Sec. 2.5 focus on an infection originating in the lungs we investigate the effects of pre-existing kidney damage (e.g. from diabetes) on the amount and duration of lung damage during pneumonia. Studies have shown that diabetics and patients with chronic kidney disease (CKD) who contract health care-associated pneumonia (HCAP) experience longer hospital stays and an increased risk of mortality ([55], [23]), so incorporating these effects into the overall model would capture important effects observed clinically.

In order to incorporate pre-existing kidney damage into the model (3.21)-(3.33) we introduce a new constant, M_{perm} , which represents the proportion of kidney function lost to the presumed chronic kidney condition. We assume that there is no pathogen infection in the kidney, so therefore $P_K(t), I_K(t), Q_K(t)$, and $C_K(I_K(t))$ are equal to 0 for all t . Thus we can simplify equation (3.28) to:

$$\frac{dM_K}{dt} = \phi(O_L - O_{L,healthy}) - \alpha_K M_K. \quad (3.34)$$

In the case of pre-existing kidney damage, if the infection is cleared, and the kidneys begin to recover, instead of recovering to $M_K = 0$, M_K will approach the long-term damage value, M_{perm} . Thus, we modify Equation (3.34) to:

$$\frac{dM_K}{dt} = \phi(O_L - O_{L,healthy}) - \alpha_K (M_K - M_{perm}). \quad (3.35)$$

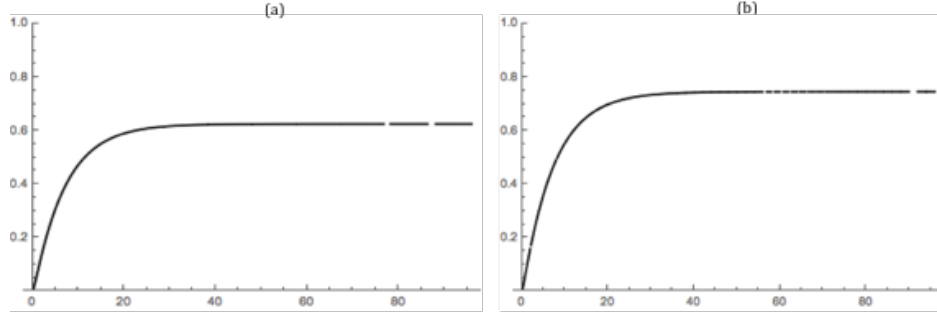


Figure 3.4: Plots of lung tissue dysfunction, $M_L(t)$, vs. time (hr). Plot (a) represents lung tissue damage for Patient 1, with no pre-existing kidney damage, modeled by the single-organ model from Section 2. Plot (b) represents lung tissue damage for Patient 2, with pre-existing kidney damage modeled using the multi-organ damage model described in Section 3.

To determine the effects of kidney dysfunction on pneumonia severity, we compare two patients. Patient 1 has no pre-existing kidney damage and is modeled using the single-organ model from Chapter 2. Patient 2 has a positive $M_{perm} = 0.2$, indicating pre-existing kidney damage, and is modeled using the multi-organ damage equations. For the lung equations for both patients (3.21)-(3.24), we use the same parameters from Tables 2.1 and 2.3, with initial pathogen load, $P_{L,0} = 100$ and $I_{L,0} = Q_{L,0} = M_{L,0} = 0$.

For the kidney equations (3.25)-(3.28) for Patient 2, we duplicate the parameters from above, with $P_{K,0} = I_{K,0} = Q_{K,0} = M_{K,0} = 0$. Parameters for the linkage terms are listed in Table 3.1. Note: in order to ensure that our hypothesis: $0 \leq M_K \leq 1$ holds, we must impose the following conditions on our Eqn. 3.35 parameters:

$$0 \leq \frac{\phi_{O_{L,healthy}}}{\alpha_K} \leq 1 - M_{perm}$$

In order to determine the severity of lung tissue damage, we take the average M_K for each patient over the course of the experiment ($0 \leq t \leq 96$) by integrating as below:

$$M_{L,avg} = \frac{1}{96} \int_0^{96} M_L(t) dt,$$

allowing us to compare lung function between patients.

Table 3.1: Parameter values for the lung-kidney damage linkage terms used in the numerical demonstration in Section 3.3.

Parameter	Description (<i>units</i>)	Model Equation	Value
η	Rate of immune responder activation due to creatinine in lungs (I_L -cells/mg/dL/min)	(3.22)	1.0
H	Saturation constant for immune responder activation due to creatinine	(3.22)	10.0
ω	Rate of lung damage due to the presence of hypoxemia (M -cells/mmHg/min)	(3.24)	2×10^{-6}
$O_{L,healthy}$	Healthy P_aO_2 (mmHg)	(3.24),(3.29)	100
ϕ	Rate of kidney damage due to hypoxia (M_K -cells/mmHg/min)	(3.28)	4.0×10^{-4}
M_{perm}	Permanent proportion of kidney dysfunction (<i>unitless</i>)	(3.28)	0.2
O_{insp}	F_iO_2 (mmHg)	(3.29)	0.2
ψ	Rate of creatinine removal by active immune cells from the lungs (W_L -cells/ I_L -cell/min)	(3.30)	0.01
R	Normal creatinine output from the liver and other auxiliary organs (mg/dL)	(3.31)	1.5
ρ	Rate of additional creatinine output from the lungs (mg/dL/min)	(3.31)	0.1
$W_{max,0}$	Maximum creatinine concentration that can be processed by fully-functional kidneys (mg/dL/min)	(3.32)	2

The results of the simulation are shown in Figure 3.4. Plot (a) models the proportion of lung dysfunction over time for Patient 1, while plot (b) models the lung dysfunction vs. time for a Patient 2. Patient 1 had a $M_{L,avg}$ value of 0.58, corresponding to LIS of 2 (i.e. moderate lung damage) a Patient 2 had $M_{L,ave} = 0.68807$, corresponding to an LIS score of 3. Since a LIS score of 2.5 or higher is indicative of Acute Respiratory Distress Syndrome (ARDS), a state of severe lung dysfunction that has a high mortality rate ([37], [34]). Since, as in Section 2.5.5, these parameters were estimated and are not necessarily biologically accurate, the results of this experiment do not necessarily indicate that pre-existing kidney damage is a precursor to ARDS. Rather, by producing two significantly different lung damage outcomes, this example illustrates the importance of incorporating the effects of multiple organ damage in predicting patient outcomes.

Chapter 4

Conclusion

We have presented a differential equations model of pathogen-induced inflammatory tissue damage, first in a single-organ system caused by the active immune response to a pathogen threat. Expanding this model, we incorporate cascading lung-kidney damage caused both by the inflammatory response and by feedback effects caused by decreased arterial oxygen pressure and circulating creatinine. We have demonstrated through numerical examples the key properties of both models, including immunological memory, and the potential of the model to be used as a tool to compare treatment options and investigate the effects of pre-existing damage on patient outcomes.

While the current multi-organ damage model has specific linkage terms for lung and kidney damage, the general structure of the model allows for the possibility to incorporate other relevant organ systems and their interdependencies. Of particular interest for future study would be the liver or heart, as the functionality of both organs is interdependent on the function of the kidneys and lungs and they play an important role in sustaining human life. Furthermore, though our numerical experiments have thus far focused on modeling pneumonia, our model allows for the possibility for the pathogen to originate in any organ system included in the model. Ultimately, this model can be expanded to incorporate the effects of sepsis, a condition characterized by a system-wide inflammatory response that is often fatal [7].

Our model assumes that tissue damage in the lungs and kidneys is caused only by the inflammatory response to pathogen or creatinine and hypoxia or hyperoxia. However, there are a number

of other factors that contribute to organ dysfunction. Especially relevant to this model is damage caused by bacterial exotoxins and drug use. Bacterial exotoxins are released by some pathogen species upon entering the body and can cause dysfunction in one of two ways: either by directly damaging organ tissue, or by provoking an active immune response ([46], [12]). Furthermore, these exotoxins can remain in the body even when the pathogen is cleared, so they must be studied and modeled separately from the current investigation [46]. Many of the treatment options investigated in this study, particularly antibiotics and NSAIDs, are processed by the kidneys. When these drugs accumulate in the kidneys, they have been shown to cause kidney damage in the form of acute tubular necrosis, and these effects are compounded when the NSAIDs and penicillin-type antibiotics are combined ([41], [36]). Therefore, future investigations into treatment options must also take into account the nephrotoxic effects of a particular drug.

Finally, our model assumes that tissue damage is entirely reparable. However, when inflammation is left uncontrolled, the release of reactive oxygen species can cause severe cell damage which can become irreparable [29]. Furthermore, the presence of scar tissue in certain organs can impede function, causing more damage [25]. Therefore, a future goal of this research will be to incorporate irreparable damage.

Bibliography

- [1] A. Alex and D. Painter. Incorporating bacterial toxins into a mathematical model of host-pathogen dynamics. 2016.
- [2] D.P. Basile, M.D. Anderson, and T.A. Sutton. Pathophysiology of acute kidney injury. *Compr. Physiol.*, 2(2):1303–1353, 2012.
- [3] A. Brandwood, K. Noble, and K. Schindhelm. Phagocytosis of carbon particles by macrophages in vitro. *Biomaterials*, 13(9):646–648, 1992.
- [4] L. Caudill and B. Lawson. A hybrid agent-based and differential equations model for simulating antibiotic resistance in a hospital ward. In R. Pasupathy, S.-H. Kim, A. Tolk, R. Hill, and M. Kuhl, editors, *Proceedings of the 2013 Winter Simulation Conference*, pages 1419–1430, Piscataway, NJ, December 2013. IEEE.
- [5] L. Caudill and B. Lawson. A unified inter-host and in-host model of antibiotic resistance and infection spread in a hospital ward. *J. Theor. Biol.*, 421:112–126, 2017.
- [6] Lester Caudill. A single-parameter model of the immune response to bacterial invasion. *Bulletin of Mathematical Biology*, 75(9):1434–1449, 2013.
- [7] Centers for Disease Control and Prevention. *Making Healthcare Safer: Think Sepsis. Time Matters.*, August 2016.
- [8] A. Clatworthy, E. Pierson, and D. Hung. Targeting virulence: a new paradigm for antimicrobial therapy. *Nature Chem. Biol.*, 3(9):541–548, 2007.

- [9] T. M. Cunha, Jr. W. A. Verri, J. S. Silva, S. Poole, F. Q. Cunha, and S. H. Ferreira. A cascade of cytokines mediates mechanical inflammatory hypernociception in mice. *Proceedings of the National Academy of Sciences of the United States of America*, 102(5):1755–1760, 2004.
- [10] M. Darmon, F. Schortgen, R. Leon, S. Moutereau, J. Mayaux, F. DiMarco, J. Devaquet, C.B. Buisson, and L. Brochard. Impact of mild hypoxemia on renal function and renal resistive index during mechanical ventilation. *Intensive Care Med.*, 35:1031–1038, 2009.
- [11] Charles A Dinarello. Proinflammatory cytokines. *Chest*, 118(2):503–508, 2000.
- [12] César Echeverria, Ignacio Montorfano, Pablo Tapia, Claudia Riedel, Claudio Cabello-Verrugio, and Felipe Simon. Endotoxin-induced endothelial fibrosis is dependent on expression of transforming growth factors $\beta 1$ and $\beta 2$. *Infection and Immunity*, 82(9):3678–686, 2014.
- [13] K.D. Elgert. *Immunology 2e*. Wiley-Blackwell, New York, 2009.
- [14] S. Faubel. Pulmonary complications after acute kidney injury. *Advances in Chronic Kidney Disease*, 15(3):284–296, 2008.
- [15] H. Felise, H. Nguyen, R. Pfuetzner, K. Barry, S. Jackson, M.-P. Blanc, P. Bronstein, T. Kline, and S. Miller. An inhibitor of Gram-negative bacterial virulence protein secretion. *Cell Host and Microbe*, 4:325–336, 2008.
- [16] MJ Fine, JJ Orloff, D Arisumi, GD Fang, VC Arena, BH Hanusa, VL Yu, DE Singer, and WN Kapoor. Prognosis of patients hospitalized with community-acquired pneumonia. *American Journal of Medicine*, 88:1–8, 1990.
- [17] W. Dana Flanders, Gary Tucker, Anusha Krishnadasan, Debra Martin, Eric Honig, and William M. McClellan. Validation of the pneumonia severity index. *Journal of General Internal Medicine*, 14(6):333–340, 1999.
- [18] Centers for Disease Control and Prevention. National and state healthcare associated infections progress report. 2016.

- [19] J. Gabrielsson and D. Weiner. *Pharmacokinetic and Pharmacodynamic Data Analysis 3e*. Swedish Pharmaceutical Society, Stockholm, Sweden, 2000.
- [20] G. Geske, R. Wezeman, A. Siegel, and H. Blackwell. Small molecule inhibitors of bacterial quorum sensing and biofilm formation. *J. Am. Chem. Soc.*, 127:12762–12763, 2005.
- [21] V.H. Haase. Mechanism of hypoxia responses in renal tissue. *Journal of the American Society of Nephrology*, 74:537–541, 2013.
- [22] Glenn W. Kaatz, Susan M. Seo, Vera N. Reddy, Elaine M. Bailey, and Michael J. Rybak. Daptomycin compared with teicoplanin and vancomycin for therapy of experimental staphylococcus aureus endocarditis. *Antimicrobial Agents and Chemotherapy*, 34(11):2081–2085, 1990.
- [23] Yusuke Kabeya, Akira Shimada, Nobuhiro Tsukada, Yoshihito Atsumi, and Megumu Higaki. Diabetes affects length of stay and hospital costs for elderly patients with pneumonia: An analysis of a hospital administrative database. *Tokai Journal of Experimental Clinical Medicine*, 41:203–209, 2016.
- [24] A. Kauppi, R. Nordfelth, H. Uvell, H. Wolf-Watz, and M. Elofsson. Targeting bacterial virulence: inhibitors of Type III secretion in *yersinia*. *Chem. Biol.*, 10:241–249, 2003.
- [25] Ellen C Keeley, Borna Mehrad, and Robert M Strieter. The role of fibrocytes in fibrotic diseases of the lungs and heart. *Fibrogenesis Tissue Repair*, 4(2), 2011.
- [26] Yuri Kheifetz, Moran Elishmereni, and Zvia Agur. Complex pattern of interleukin-11-induced inflammation revealed by mathematically modeling the dynamics of c-reactive protein. *J Pharmacokinetic Pharmacodyn*, 41:479–491, 2014.
- [27] C.L. Klein, T.S. Hoke, W.F. Fang, C.J. Altmann, I.S. Douglas, and S. Faubel. Interleukin-6 mediates lung injury following ischemic acute kidney injury or bilateral nephrectomy. *Kidney International*, 74:901–909, 2008.
- [28] Rukmini Kumar, Gilles Clermont, Yoram Vodovotz, and Carson C. Chow. The dynamics of acute inflammation. *Journal of Theoretical Biology*, 230(2):145–55, 2004.

- [29] Yunlong Lei, Kui Wang, Longfei Deng, Yi Chen, Edouard C. Nice, and Canhua Huang. Redox regulation of inflammation: Old elements, a new story. *Medicinal Research Reviews*, 35(2):306–340, 2014.
- [30] M.-C. Li and S.H. He. Il-10 and its related cytokines for treatment of inflammatory bowel disease. *World J. Gastroenterol.*, 10(5):620–625, 2004.
- [31] E Louis, D Franchimont, A Piron, Y Gevaert, N Schaaf-Lafontaine, S Roland, P Mahieu, M Malaise, D DeGroote, R Louis, and J Belaiche. Tumor necrosis factor (tnf) gene polymorphism influences tnf-alpha production in lipopolysaccharide (lps)-stimulated whole blood cell culture in healthy humans. *Clinical and Experimental Immunology*, 113:401–406, 1998.
- [32] W.J. Mach, A. R. Thimmesch, J.T. Pierce, and J.D. Pierce. Consequences of hyperoxia and the toxicity of oxygen in the lungs. *Nursing Research and Practice*, pages 1–7, 2011.
- [33] K.L McCance and S.E. Huethe, editors. *Pathophysiology: The Biologic Basis for Disease in Adults and Children*. Mosby, 7 edition, 2014.
- [34] G. Umberto Meduri, Stacey Headley, Gary Kohler, Frankie Stentz, Elizabeth Tolley, Reba Umberger, and Kenneth Leeper. Persistent elevation of inflammatory cytokines predicts a poor outcome in ards. *Chest*, 107(1):1062–1073, 1995.
- [35] M. Monchi, F. Bellenfant, A. Cariou, L.-M. Joly, D. Thebert, I. Laurent, J.-F. Dhainaut, and F. Brunet. Early predictive factors of survival in the acute respiratory distress syndrome: a multivariate analysis. *Am. J. Respir. Crit. Care Med.*, 158:1076–1081, 1998.
- [36] JP Morin, JP Fillastre, and B Olier. Antibiotic nephrotoxicity. *Chemioterapia*, 3(1):33–40, 1984.
- [37] J. Murray, M. Matthay, J. Luce, and M. Flick. An expanded definition of the adult respiratory distress syndrome. *Am. Rev. Respir. Dis.*, 138:720–723, 1988.

- [38] D. Nelson, Z. Tu, C. Soldevila-Pico, M. Abdelmalek, H. Zhu, Y. Xu, R. Cabrera, C. Liu, and G. Davis. Long-term Interleukin 10 therapy in chronic Hepatitis C patients has a proviral and anti-inflammatory effect. *Hepatology*, 38(4):859–868, 2003.
- [39] W. Ouyang, S. Rutz, N.K. Crellin, P.A. Valdez, and S.G. Hymowitz. Regulation and functions of the il-10 family of cytokines in inflammation and disease. *Annu. Rev. Immunol.*, (29):71–109, 2011.
- [40] M. Paats, I. Bergen, W. Hanselaar, E. Groeninx van Zoelen, H. Hoogsteden, R. Hendriks, and M. van der Eerden. Local and systemic cytokine profiles in nonsevere and severe community-acquired pneumonia. *European Respiratory Journal*, 41:1378–1385, 2013.
- [41] YO Pospishil and TM Antonovych. Nsaids associated nephropathy. *Polish Journal of Pathology*, 49(1):35–39, 1998.
- [42] D. Rasko and V. Sperandio. Anti-virulence strategies to combat bacteria-mediated disease. *Nature Rev. Drug Discovery*, 9:117–128, 2010.
- [43] K. Reich, C. Garbe, V. Blaschke, C. Maurer, P. Middel, G. Westphal, U. Lippert, and C. Neumann. Response of psoriasis to interleukin-10 is associated with suppression of cutaneous Type 1 inflammation, downregulation of the epidermal interleukin-8/cxcr2 pathway and normalization of keratinocyte maturation. *J. Investig. Dermatol.*, 116(2):319–329, 2001.
- [44] A. Reynolds, J. Rubin, G. Clermont, J. Day, Y. Vodovotz, and G. Ermentrout. A reduced mathematical model of the acute inflammatory response: I. derivation of model and analysis of anti-inflammation. *J. Theor. Biol.*, 242(1):220–236, 2006.
- [45] Angela Reynolds, Jonathan Rubin, Gilles Clermont, Judy Day, Yoram Vodovotz, and G. Bard Ermentrout. A reduced mathematical model of the acute inflammatory response: I. derivation of model and analysis of anti-inflammation. *Journal of Theoretical Biology*, 242(1):220–36, 2006.

- [46] Cristina Risco and Pedro Pinta da Silva. Cellular functions during activation and damage by pathogens: Immunogold studies of the interaction of bacterial endotoxins with target cells. *Microscopy Research and Technique*, 31(2):141–158, 1995.
- [47] M. Sarac, J. Peinado, S. Leppla, and I. Lindberg. Protection against anthrax toxemia by hexa-D-arginine *in vitro* and *in vivo*. *Infection and Immunity*, 73(1):602–605, 2004.
- [48] S. Schreiber, R. Fedorak, O. Nielsen, G. Wild, C. Williams, S. Nikolaus, M. Jacyna, b. Lashner, A. Gangl, P. Rutgeerts, K. Isaacs, S. van Deventer, J. Koningsberger, M. Cohard, A. LeBeaut, and S. Hanauer. Safety and efficacy of recombinant human interleukin 10 in chronic active Crohn’s disease. *Gastroenterology*, 119:1461–1472, 2000.
- [49] R.D. Scott. The direct medical costs of healthcare-associated infections in u.s. hospitals and the benefits of prevention. 2009.
- [50] R.A. Sharkey, E.M.T. Mulloy, and S.J O’Neil. Acute effects of hypoxaemia, hyperoxaemia, and hypercapnia on renal blood flow in normal and renal transplant subjects. *European Respiratory Journal*, 12:653–657, 1998.
- [51] M. Steinhauser, C. Hogaboam, S. Kunkel, N. Lukacs, R. Strieter, and T. Standiford. Il-10 is a major mediator of sepsis-induced impairment in lung antibacterial host defense. *J. Immunol.*, 162:392–399, 1999.
- [52] MD Steven M. Opal and MD Vera A. DePalo. Anti-inflammatory cytokines. *Chest*, 117(4):1162–1172, 2000.
- [53] T. Sursal, DJ Stearns-Kurosawa, K. Itagaki, SY Oh, S. Kurosawa, and CJ Hauser. Plasma bacterial and mitochondrial dna distinguish bacterial sepsis from sterile systemic inflammatory response syndrome and quantify inflammatory tissue injury in nonhuman primates. *Shock*, 39(1):55–62, 2013.
- [54] L. Ternent, R. Dyson, A.-M. Krachler, and S. Jabbari. Bacterial fitness shapes the population dynamics of antibiotic-resistant and susceptible bacteria in a model of combined antibiotic and anti-virulence treatment. *J. Theor. Biol.*, 372:1–11, 2015.

- [55] Diego Viasus, Carolina Garcia-Vidal, Josep M. Cruzado, Jordi Adamuz, Ricard Verdaguier, Frederic Manresa, Jordi Dorca, Frencesc Gudiol, and Jordi Carratala. Epidemiology, clinical features, and outcomes of pneumonia in patients with chronic kidney disease. *Nephrology Dialysis and Transplant*, 26:2899–2906, 2011.
- [56] J.-L. Vincent, R. Moreno, J. Takala, S. Willatts, A. De Mendonca, H. Bruining, C. Reinhart, P. Suter, and L. Thijs. The SOFA (Sepsis-related Organ Failure Assessment) score to describe organ dysfunction/failure. *Intensive Care Med.*, 22:707–710, 1996.
- [57] D. Wallach, T.-B. Kang, and A. Kovalenko. Concepts of tissue injury and cell death in inflammation: A historical perspective. *Nature Reviews Immunology*, 14:51–59, 2014.
- [58] L. Ware and M. Matthay. The acute respiratory distress syndrome. *New England J. Med.*, 342(18):1334–1349, 2000.
- [59] A. Wheeler and G. Bernard. Acute lung injury and the acute respiratory distress syndrome: a clinical review. *Lancet*, 369:1553–1565, 2007.
- [60] H. Wu, Z. Song, M. Hentzer, J. Andersen, S. Molin, M. Givskov, and N. Hoiby. Synthetic furanones inhibit quorum-sensing and enhance bacterial clearance in *pseudomonas aeruginosa* lung infection in mice. *J. Antimicrob. Chemother.*, 53:1054–1061, 2004.
- [61] Kai Yang, Hu Zeng Sharad Shrestha, Peer W.F. Karmaus, Geoffrey Neale, Peter Vogel, David A. Guertin, Richard F. Lamb, and Hongbo Chi. T cell exit from quiescence and differentiation into th2 cells depend on raptor-mtorci-mediated metabolic reprogramming. *Immunity*, 39(6):1043–056, 2013.